Redox Biology 85 (2025) 103751

Contents lists available at ScienceDirect

Redox Biology

journal homepage: www.elsevier.com/locate/redox

Targeting Dio3 to enhance mitophagy and ameliorate skeletal muscle wasting in sepsis

Gang Wang [a,b,e,1], Ming Chen [a,b,1], Yuheng Zhang [c,1], Dacheng Wang [d], Tao Gao [a,b], Jianfeng Duan [a,b], Huimin Lu [a,b], Minhua Cheng [a,b], Yun Xu [a,b], Xiaoyao Li [a,b], Yan Wang [a,b], Ke Cao [a,b,*], Wenkui Yu [a,b,**]

[a] Department of Critical Care Medicine, Nanjing Drum Tower Hospital, Affiliated Hospital of Medical School, Nanjing University, Nanjing, 210008, China
[b] The State Key Laboratory of Pharmaceutical Biotechnology, Nanjing, 210093, China
[c] Department of General Surgery, Children's Hospital of Nanjing Medical University, Nanjing, 210008, China
[d] Department of Intensive Care Unit, Affiliated Hospital of Nanjing University of Chinese Medicine, Jiangsu province hospital of Chinese medicine, Nanjing, 210029, China
[e] Department of Emergency, The Affiliated Taizhou People's Hospital of Nanjing Medical University, Taizhou, 225300, China

A B S T R A C T

Recent studies highlight the role of skeletal muscle wasting in the sepsis-associated long-term mortality. Despite clinical recommendations for increased protein intake to counteract muscle wasting, the outcomes have been suboptimal, suggesting that anabolic resistance should be considered in addition to nutritional support. Emerging evidence suggests that impaired mitophagy hampers anabolic processes in skeletal muscle, exacerbating muscle wasting in sepsis. Furthermore, thyroid hormone (TH), which is essential for both anabolism and mitophagy, is locally inactivated by type 3 Deiodinase (Dio3) at the onset of sepsis, potentially disrupting mitophagy and contributing to anabolic resistance. Here we demonstrate that local hypothyroidism is a key factor impairing mitophagy in skeletal muscle during early sepsis, leading to metabolic disturbances and muscle wasting. Dio3 knockdown preserves muscle mass, and ameliorates metabolic dysfunction via mitophagy promotion in sepsis models. Mechanistically, the knockdown of Dio3 triggers an upregulation of NRK2, facilitating the restoration of NAD salvage synthesis. This enhancement of NAD levels subsequently activates Sirtuins deacetylase, which in turn decreases PINK1 acetylation, preventing its proteolytic processing by OMA1. Therefore, targeting Dio3 offers a promising therapeutic approach to counteract sepsis-induced muscle wasting.

1. Introduction

Sepsis, a common clinical condition, is marked by a dysregulated host response to infection, leading to multiple organ failure and a high risk of mortality [1]. While the success rate of acute sepsis treatment has improved in recent years, long-term survival rates at 1–3 years remain largely unchanged [2]. Growing evidence suggests that sepsis-associated muscle wasting plays a pivotal role in affecting the long-term quality of life and prognosis of sepsis patients [3]. Consequently, researchers are increasingly focused on elucidating the mechanisms underlying sepsis-induced muscle wasting to improve long-term outcomes. While clinical nutritionists have advocated for higher protein intake to counteract muscle catabolism, recent large-scale randomized controlled trials have shown that this approach does not achieve the expected goals and may even be detrimental for patients with renal comorbidities [4,5]. These findings highlight that nutritional supplementation alone is insufficient to combat muscle wasting. Identifying effective interventions to counteract muscle wasting remains a critical research priority.

The imbalance between catabolic and anabolic processes is well-established as a primary driver of muscle wasting [6]. While most studies have concentrated on catabolism, highlighting the critical roles of inflammatory cytokines such as IL-6 and TNFα, the efficacy of anti-inflammatory therapies in mitigating muscle wasting remains controversial [7]. In contrast, anabolic resistance, another key factor in muscle wasting, has received relatively little attention. Among the factors influencing skeletal muscle metabolism, thyroid hormone (TH) is strongly linked to anabolic resistance [8]. Local hypothyroidism disrupts

* Corresponding author. Department of Critical Care Medicine, Nanjing Drum Tower Hospital, Affiliated Hospital of Medical School, Nanjing University, Nanjing, 210008, China
** Corresponding author. Department of Critical Care Medicine, Nanjing Drum Tower Hospital, Affiliated Hospital of Medical School, Nanjing University, Nanjing, 210008, China
E-mail addresses: medic_ck@126.com (K. Cao), yudrnj2@163.com (W. Yu).
[1] These authors contributed equally.

https://doi.org/10.1016/j.redox.2025.103751
Received 5 June 2025; Received in revised form 25 June 2025; Accepted 2 July 2025
Available online 3 July 2025

the activation of AKT, a crucial protein in anabolic signaling, and also impairs glucose and lipid metabolism in skeletal muscle contributing to substrate utilization deficit [9,10]. Recent studies suggest that during the early stages of sepsis, local TH activity is inactivated in skeletal muscle due to induced expression of type 3 deiodinase (Dio3) which converts T4 to the biologically inactive reverse triiodothyronine (rT3) [11]. This adaptation appears to conserve energy by reducing basal metabolic rate and prioritizing nutrients for essential organs like the liver, brain, and immune system. However, the dysregulation of the hypothalamic-pituitary-thyroid feedback axis results in sustained systemic hypothyroidism during sepsis, thereby potentially impairing tissue metabolism. Specifically, the persistent low-T3 state chronically impairs the function of skeletal muscle which is proved by a longitudinal study focusing on the muscle function of ICU survivors [12]. Moreover, local hypothyroidism, whether due to systemic hypothyroidism or TH resistance, is strongly linked to muscle wasting [13]. Our group has previously shown that the targeted knockdown of Dio3 in the tibialis anterior (TA) muscle of rats subjected to cecal ligation and puncture (CLP) model mitigates sepsis-induced metabolic dysfunction and muscle wasting [14], yet the mechanisms responsible for these effects remain to be fully elucidated.

Emerging evidence highlights the critical role of TH in mitochondrial quality control (MQC), regulating processes such as mitochondrial biogenesis and mitophagy to sustain tissue metabolic equilibrium [15]. Concurrently, hypothyroidism-associated skeletal muscle developmental impairments are directly correlated with mitochondrial dysfunction [16]. Notably, recent findings emphasize the critical function of mitophagy in preventing muscle wasting [17]. Impaired mitophagy has been associated with defective muscle differentiation, while its promotion mitigates sepsis-related muscle loss [18,19]. In sepsis, however, a mismatch between mitophagy and mitochondrial damage has been observed, which may potentially contribute to persistent muscle wasting [20]. Given the pivotal role of the TH axis in regulating mitochondrial quality control, we hypothesize that disrupted mitophagy could be associated with sepsis-induced local hypothyroidism, collectively contributing to muscle wasting.

Based on the above, we speculate that in the early stages of sepsis, induction of Dio3 leads to local hypothyroidism in skeletal muscle, affecting the initiation of mitophagy and primarily contributing to metabolic disarray and muscle wasting. In this work, utilizing metabolomics, ChIP, and co-immunoprecipitation (Co-IP) experiments, we demonstrate that restoring local TH activity by knocking down Dio3 maintains muscle mass and metabolic homeostasis by enhancing mitophagy, an effect mediated by preventing the degradation of PTEN-induced kinase 1 (PINK1), as confirmed in both in vivo and in vitro models.

2. Results

2.1. Local hypothyroidism impedes mitophagy in skeletal muscle during sepsis

As a specialized form of autophagy, mitophagy maintains cellular homeostasis by selectively degrading damaged mitochondria [21]. Current research categorizes mitophagy into two primary pathways: The PINK1/E3 Ubiquitin-Protein Ligase Parkin (Parkin)-dependent pathway and the receptor-mediated pathway. Under physiological conditions, PINK1 is cleaved by inner mitochondrial membrane (IMM) proteases and subsequently released into the cytosol for degradation [22]. However, during acute stress, the import of PINK1 into the IMM is inhibited, leading to its accumulation on the outer mitochondrial membrane (OMM). This accumulation recruits and activates Parkin, which facilitates the engulfment of damaged mitochondria by the autophagosomal membrane and their subsequent clearance [23]. The receptor-mediated pathway, involving proteins such as BCL2 Interacting Protein 3 (BNIP3) and FUN14 Domain Containing 1 (FUNDC1), can recruit the autophagosomal membrane protein Microtubule-Associated Protein 1 Light Chain 3B (LC3B) to initiate mitophagy independently [24].

Emerging evidence underscores the critical role of mitophagy in counteracting muscle wasting [25]. In spite of this, recent investigations imply that mitophagy may be insufficiently activated in the skeletal muscle of mice during the early stages of sepsis [20]. To substantiate this observation, we established a sepsis model in rat using CLP and collected skeletal muscle samples 24 h post-procedure. Transmission electron microscopy (TEM) of septic muscle samples revealed substantial mitochondrial damage, characterized by hallmarks as discontinuity of the mitochondrial membrane, disordered mitochondrial cristae structure, or vacuolar-like changes (Fig. 1A and B) [26]. Despite this, little increase in mitochondrial autophagosomes was observed. Immunoblotting showed that autophagy biomarkers, including the *p*-ULK1 to ULK1 ratio and the LC3B II to LC3B I ratio, were significantly increased compared to the sham group, while P62 expression was decreased (Fig. 1C). The mitophagy biomarkers BNIP3, FUNDC1, and PINK1 were significantly downregulated, while Parkin expression remained unchanged (Fig. 1D). To further evaluate mitophagy levels, we performed dual immunofluorescence staining for LC3B and Outer Mitochondrial Membrane 20 (Tom20) on the same samples mentioned above. LC3B, indicative of the autophagosomal membrane, and Tom20, specific for the OMM, were utilized to assess colocalization and serve as a mitophagy indicator. The results demonstrated that the ratio of colocalization of the double-positive area to Tom20 positive area was significantly lower in muscles of CLP group rats, suggesting an impairment of mitophagy (Fig. 1E). To further clarify this phenomenon, we conducted the same dual immunofluorescence on skeletal muscle biopsies from septic patients. Findings showed no significant LC3B expression differences between acute and recovery phases, while Tom20 expression was diminished in the acute phase. Additionally, mitophagy levels were markedly reduced in the acute phase versus the recovery phase (Fig. 1F and S1A).

Considering THs as key modulators of mitophagy, we performed a correlation analysis of peripheral T3, T4, fT3, fT4, TSH and rT3 levels with mitophagy levels mentioned above. The results revealed a significant negative correlation between mitophagy data and rT3 levels, indicating that reduced TH activity contributes to mitophagy impairment. (Fig. 1G and S1B). Previous research suggests that Dio3 predominantly mediates the reduction of the TH axis in skeletal muscle during sepsis. Our findings align with this, demonstrating a significant upregulation of Dio3 in skeletal muscle 24 h post-CLP (Fig. 1H). Concurrently, TH-associated genes exhibit substantial downregulation (Fig. S1C). Considering that Dio3 inversely correlates with local TH activity, we further stratified biopsy samples into high- and low-Dio3 groups based on Dio3 IHC expression levels. Results from IHC staining for mitophagy biomarkers on the same biopsy samples demonstrated significantly higher expression of BNIP3, FUNDC1, and PINK1 in the low-Dio3 group (Fig. 1I and J). Additionally, Spearman's correlation analysis revealed a strong but negative correlation between Dio3 and the expressions of BNIP3 and PINK1, while no significant correlation was observed with FUNDC1 (Fig. 1K). Collectively, these findings indicate that mitophagy in skeletal muscle is inhibited during early sepsis, which is potentially associated with decreased local TH activity.

2.2. Dio3 knockdown promotes mitophagy both in vivo and in vitro

To restore TH activity in skeletal muscle, we employed adeno-associated virus (AAV) to specifically knock down Dio3 expression in the TA muscle of rats. Immunoblotting results revealed that 48 h post-CLP, Dio3 was significantly upregulated in the TA muscle of the CLP group, coincident with reduced expression of *THRα, THRβ, MCT8,* and *MCT10*, suggesting decreased TH activity. In contrast, Dio3 knockdown effectively restored local TH activity (Fig. 2A and S2A). To directly assess mitophagy levels, we performed dual immunofluorescence staining for LC3B and Tom20 on rat TA muscles as mentioned above.

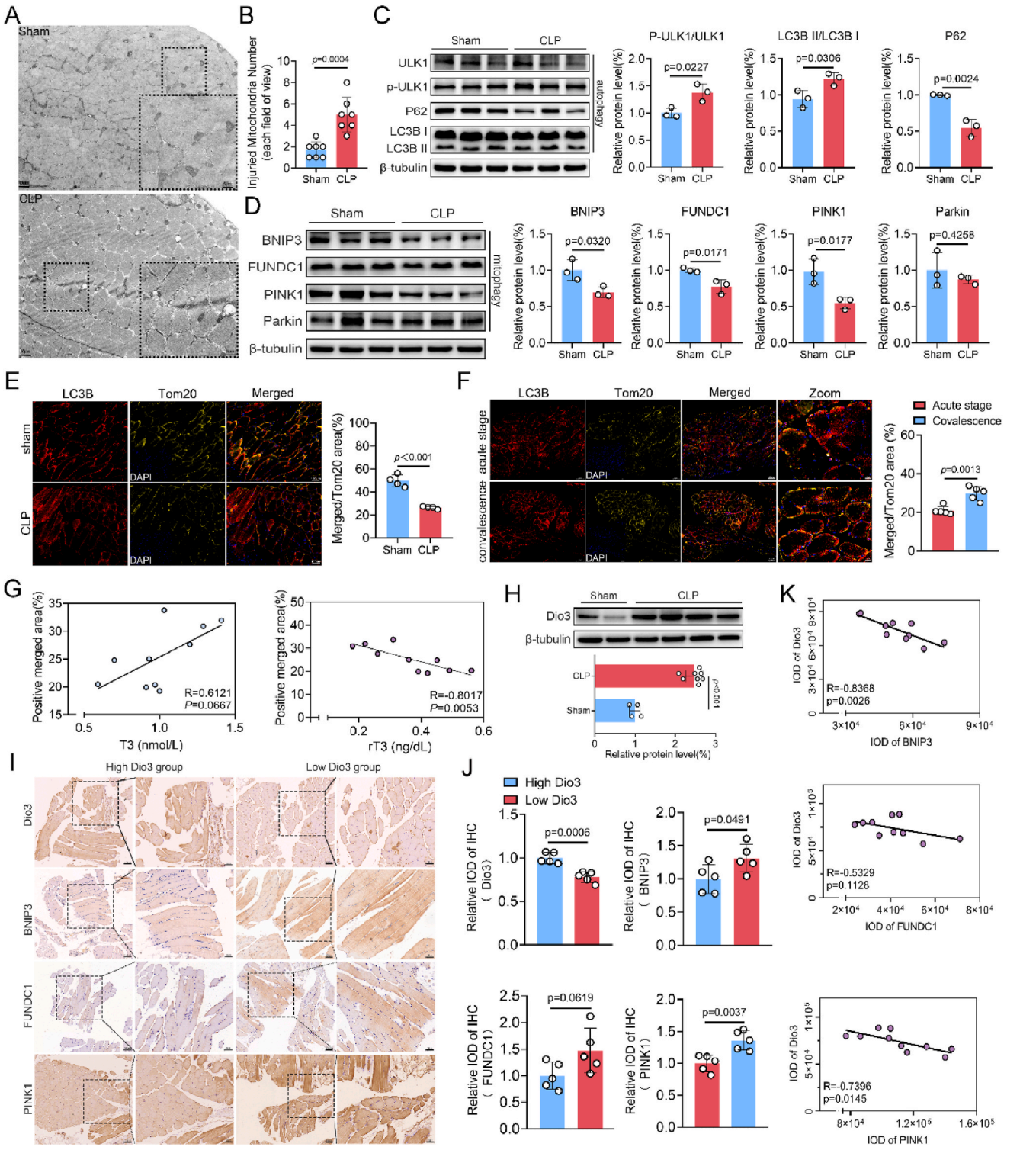

Fig. 1. Local hypothyroidism impedes mitophagy in skeletal muscle during sepsis. (A) Representative TEM images of skeletal muscles from sham or 24h-CLP rats (scale bar: 5 μm). (B) Quantification of mitochondrial damage in (A), assessed by mitochondrial injury hallmarks listed in the Methods section (n = 7). (C) Immunoblots of autophagy-related proteins (ULK1, *p*-ULK1, P62, LC3B I/II) in TA muscles from sham or 24h-CLP rats, with quantification. (D) Immunoblots of mitophagy-related proteins (BNIP3, FUNDC1, PINK1, Parkin) in TA muscles from sham or 24h-CLP rats, with quantification (n = 3). (E) Immunofluorescence of LC3B (red) and Tom20 (golden) in rat muscle samples (as in C; scale bar: 100 μm; n = 4). (F) Immunofluorescence of LC3B (red) and Tom20 (golden) in septic patient muscle biopsies: acute stage (≤1 week post-admission, n = 5) vs. convalescence (pre-discharge, n = 5; scale bar: 100 μm). (G) Spearman's correlation between serum T3, rT3 and mitophagy data from (F, n = 10). (H) Immunoblots of Dio3 expression in skeletal muscles from sham or 24h-CLP rats, with quantification. (I) Representative IHC staining of Dio3, BNIP3, FUNDC1, and PINK1 in septic patient muscle biopsies, stratified by Dio3 expression (scale bars: 50 μm, 100 μm; n = 5). (J) Quantification of IHC staining in (I). (K) Spearman's correlation between BNIP3, FUNDC1, PINK1, and Dio3 levels (n = 10). To ensure blot comparability, identical sample volumes were loaded for both phospho- and total-protein detection, with all membranes probed for β-tubulin as loading control. Data are mean ± SD. *P < 0.05; NS, not significant. (B, C, D, E, F, H, J): Two-tailed unpaired *t*-test or Mann-Whitney test; (G, K): Spearman's correlation.

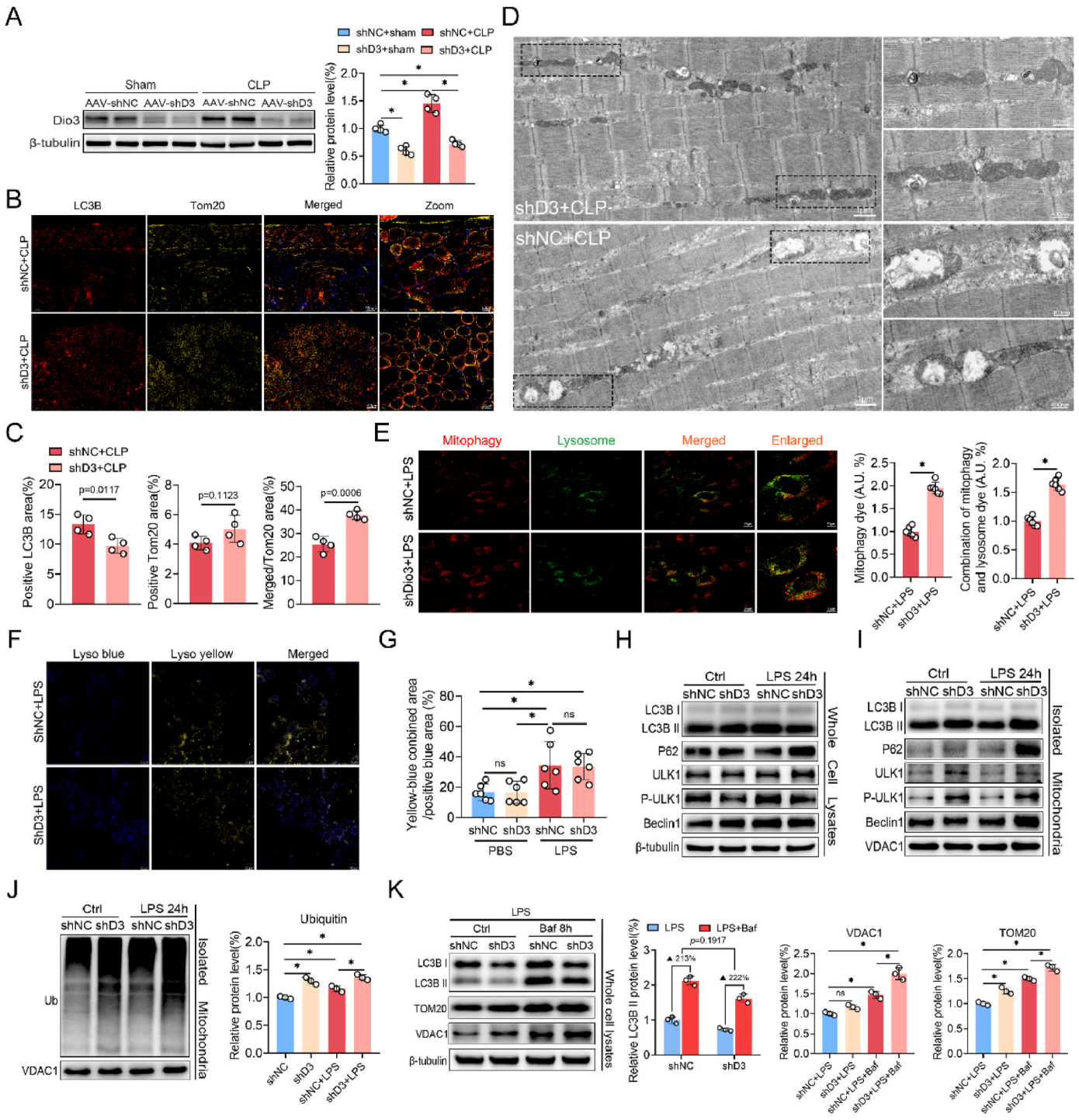

Fig. 2. Dio3 knockdown promotes mitophagy both in vivo and in vitro. (A) Representative Dio3 immunoblots in TA muscles from rats of indicated groups (shNC+sham, shD3+sham, shNC+CLP, shD3+CLP) with quantification (n = 4). (B) Immunofluorescence of LC3B (red) and Tom20 (golden) in TA muscles of shNC+CLP and shD3+CLP rats (n = 4; scale bars: 20 μm, 100 μm). (C) Quantification of (B). (D) TEM images of mitochondria morphology in TA muscles from shNC+CLP and shD3+CLP rats with enlarged views representing mitophagosomes in shD3+CLP group which are less frequently observed in shNC+CLP group (n = 6; scale bars: 1 μm, 400 nm). (E) Mitophagy assessment in C2C12 myoblasts transfected with shNC or shDio3 and treated with 100 μg/mL LPS. Representative images show Mtphagy dye (red), Lyso dye (green), merged and enlarged views (n = 6; scale bars: 50 μm, 100 μm). (F) Lysosomal acidification rates detected by LysoSensor probe in shNC+LPS and shD3+LPS cells (blue: neutral lysosomes; yellow: acidified lysosomes; scale bar: 20 μm). (G) Quantification of (F, n = 6). (H) Immunoblots of autophagy-related proteins (ULK1, *p*-ULK1, P62, LC3B I/II, Beclin1) in whole-cell lysates of C2C12 myoblasts transfected with shNC or shDio3 and treated with or without LPS (100 μg/mL). (I) Immunoblots of autophagy-related proteins (as in H) in mitochondrial fractions under the same conditions. (J) Immunoblots of ubiquitin levels in mitochondrial fractions (conditions as in H). (K) Immunoblots of LC3B I/II, Tom20, and VDAC1 in shNC or shD3 myoblasts treated with LPS ± bafilomycin A1 (40 nM, 8 h). β-tubulin (whole-cell and cytosol loading control); VDAC1 (mitochondrial loading control). To ensure blot comparability, identical sample volumes were loaded for both phospho- and total-protein detection, with all membranes probed for β-tubulin as loading control. Data are mean ± SD. *P < 0.05; NS, not significant. (C, E): Unpaired two-tailed *t*-test; (A, G, J, K): One-way ANOVA with Tukey's post hoc test.

Following CLP modelling, LC3B-positive areas significantly increased in the shNC+CLP group, while Tom20 positive areas showed no statistical difference compared to the shD3+CLP group. However, the dual positive area ratio indicative of mitophagy levels were markedly higher in the shD3+CLP group (Fig. 2B–C). Furthermore, TEM results revealed that mitophagosomes were more frequently observed in the shD3+CLP group compared to the shNC+CLP group (Fig. 2D).

In vitro study, targeted Dio3 knockdown in C2C12 cells using lentivirus was validated (Fig. S2C). A pH-sensitive mitophagy probe indicated increased mitophagy through enhanced red fluorescence intensity and increased double-positive regions for mtphagy and lyso dyes was used for evaluating mitophagy levels. The shD3 group exhibited enhanced mitophagy compared to the shNC group (Fig. S2D). Furthermore, the level of mitophagy in the shD3+LPS group was significantly elevated relative to the shNC+LPS group (Fig. 2E). Contrary to in vivo findings, LPS stimulation slightly elevated mitophagy levels in vitro, a phenomenon that may be attributed to the inability of LPS to fully replicate the complex pathophysiological features of sepsis. Given that lysosomal acidification rate is also a critical factor in promoting mitophagy [27], we measured the lysosomal acidification levels in each group using a pH-sensitive lysosomal probe. The results demonstrated that the LPS-treated groups exhibited significantly elevated lysosomal acidification rates compared to both the shNC and shD3 groups. However, no significant difference was observed between the shNC+LPS and shD3+LPS groups (Fig. 2F and G and S2E). Additionally, Dio3 knockdown enhanced the expression of autophagy-related proteins such as LC3B, P62, ULK1, and Beclin1 at the mitochondrial level while suppressing their global expression (Fig. 2H and I, S2F, and S2G). Enhanced mitochondrial ubiquitination was observed following Dio3 knockdown (Fig. 2J). Moreover, upon inhibition of lysosomal degradation with bafilomycin A1 (BafA1), LPS stimulation significantly increased LC3B-II levels in all experimental groups. However, the magnitude of this increase showed no significant difference between the shNC+LPS and shD3+LPS groups, indicating that the overall increase in autophagic flux was comparable. In contrast, within the BafA1-treated shD3+LPS group, the accumulation of Tom20 and VDAC1 was markedly more pronounced, suggesting a specific enhancement of mitophagic flux (Fig. 2K). Collectively, these results demonstrate that Dio3 knockdown enhances mitophagy both in vivo and in vitro.

2.3. *Dio3 knockdown mitigates septic muscle wasting by preserving mitochondrial function and restoring lipid metabolic capacity*

Exogenous T3 supplementation has been shown to protect mitochondrial function across various diseases. Unlike traditional supplementation strategies, our targeted Dio3 knockout has successfully restored tissue TH activity. Yet, the potential of this method to safeguard mitochondrial function has not been documented. TEM post-CLP revealed mitochondrial swelling and cristae damage in both the intermyofibrillar and subsarcolemmal regions of skeletal muscle. Dio3 knockdown, however, preserved mitochondrial morphology and structural integrity (Fig. 3A and S3A). To systematically evaluate the impact of Dio3 knockdown on mitochondrial energy metabolism, we conducted in vitro assessments using the Seahorse XF Cell Mito Stress Test across experimental groups. Results demonstrated that the shNC+LPS group exhibited significant decreases in core mitochondrial parameters compared to the shNC group, including basal respiration rate, ATP production capacity, and maximal respiratory capacity. Notably, Dio3 knockdown substantially reversed LPS-induced mitochondrial dysfunction, with the shD3+LPS group showing marked improvements in these metabolic indices relative to the shNC+LPS group (Fig. 3B–B).

Mitochondrial impairment is a key driver of metabolic dysregulation in sepsis [28]. During sepsis, a metabolic shift from glucose to lipid utilization is well-documented, which is a hallmark of the metabolic changes observed in this condition [29]. Our Oil Red O staining revealed a significant increase in lipid droplets in the shNC+CLP group compared to the shNC+sham group, indicating an elevated demand or impaired metabolic capacity for lipids (Fig. 3C). Furthermore, while the transcriptional levels of *CD36* remained unchanged, the expression of *Carnitine Palmitoyltransferase 1B* (*CPT1b*) - a rate limiting enzyme for lipid metabolism - as well as the expression of *Long Chain Acyl-CoA Dehydrogenase* (*LCAD*), *medium-chain Acyl-CoA Dehydrogenase* (*MCAD*), and *short-chain Acyl-CoA Dehydrogenase* (*SCAD*), significantly decreased following CLP (Fig. 3D). However, Dio3 knockdown alleviated CLP modeling induced lipid droplets accumulation and restored the expression of genes involved in lipid β-oxidation. These findings indicate that CLP modeling likely impairs skeletal muscle lipid utilization—consistent with prior clinical observations but previously lacking direct experimental validation. To test this hypothesis, we isolated mitochondria from TA muscles in each experimental group and performed Seahorse substrate oxidation stress test to evaluate CPT1-dependent metabolic function. Results demonstrated that mitochondria from the shNC+CLP group exhibited significantly reduced ADP-driven metabolic capacity toward substrates (palmitoyl-CoA/carnitine/malate) and attenuated acute responsiveness to FCCP stimulation compared to the shNC+sham controls. Crucially, Dio3 knockdown substantially rescued these CLP-induced deficits (Fig. 3E). Subsequent specific inhibition of CPT1 by etomoxir (quantified by ΔOCR calculation) revealed compromised CPT1-dependent basal metabolism and FCCP-responsive capacity in shNC+CLP group. Conversely, Dio3 knockdown significantly elevated both parameters relative to the shNC+CLP group, indicating enhanced lipid metabolism through sustained CPT1 activity (Fig. 3F). In vitro experiments further demonstrated a higher proportion of lipid-mitochondria proximity in the shD3+LPS group compared to shNC+LPS, implying enhanced spatial interaction (Fig. 3G, S3C and S3D). Previous studies confirm that mitochondria adjacent to lipid droplets exhibit augmented lipid oxidation capacity [30], indicating that Dio3 knockdown may improve lipid metabolism by enhancing mitochondrial energetic capacity, though this mechanism requires further validation. Sepsis also triggered a shift in muscle fiber composition from glycolytic fast-twitch fibers to oxidative slow-twitch fibers, which may contribute to impaired systemic glucose regulation but was reversed by Dio3 knockdown (Fig. 3H–I). Moreover, the ratios of TA weight to body weight and muscle fiber diameters were significantly improved in shD3+CLP group compared to shNC+CLP group (Fig. 3J and K, S3E and S3F). Dio3 knockdown also increased the expression of Myogenic Differentiation (*MyoD*) and Myogenin (*MyoG*), key regulators of muscle regeneration (Fig. 3L). Furthermore, the assessment of anabolic and catabolic protein markers revealed that Dio3 knockdown increased the *p*-AKT/Protein Kinase B (AKT) and *p*-mTOR/Mammalian Target of Rapamycin (mTOR) ratios, indicating enhanced anabolic processes (Fig. 3M). Forkhead Box O1 (FoxO1), a key regulator of muscle wasting in sepsis, is degraded via phosphorylation. We found that the *p*-FoxO1/FoxO1 ratio significantly increased after Dio3 knockdown, and the expression of two other major catabolic markers, Muscle Atrophy F-Box Protein (FBXO32) and Muscle-Specific RING Finger Protein 1 (TRIM63), also significantly decreased (Fig. 3N).

Collectively, these results suggest that Dio3 knockdown mitigates septic muscle wasting by preserving mitochondrial function and restoring primarily lipid metabolic capacity.

2.4. *Dio3 knockdown promotes mitophagy and anabolism in a PINK1/Parkin-dependent manner*

To elucidate the mechanism by which Dio3 knockdown promotes mitophagy and anabolism, we examined mitophagy-related protein markers in rat skeletal muscle. Although no significant increase in the expression of BNIP3 and FUNDC1 was observed following Dio3 knockdown, the expression of PINK1 and Parkin was significantly upregulated (Fig. 4A and S4A). IHC analysis further confirmed a robust increase in PINK1 expression in the shD3+CLP group compared to the shNC+CLP group (Fig. 4B). Additionally, Dio3 knockdown elevated PINK1

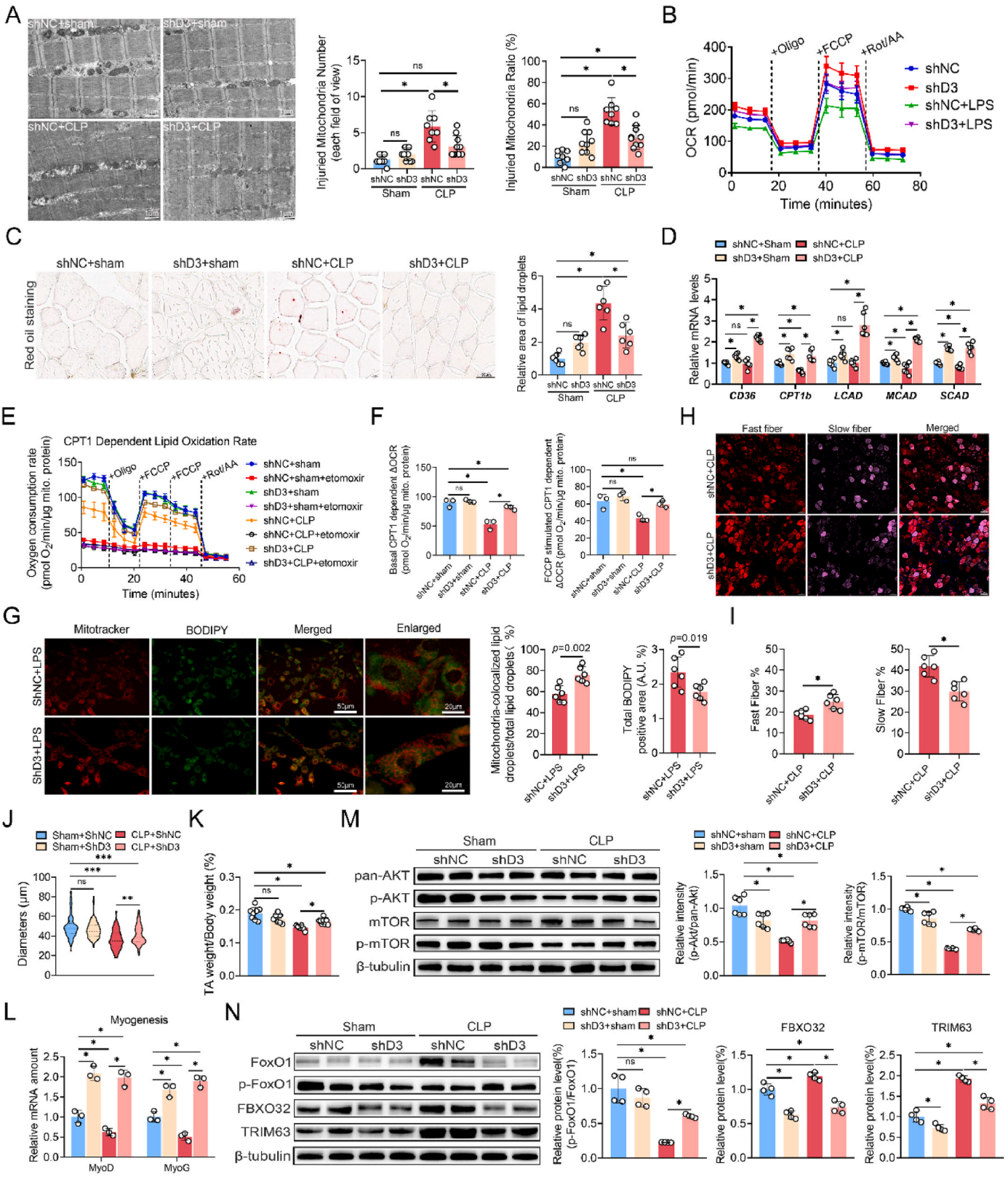

(caption on next page)

Fig. 3. Dio3 knockdown mitigates septic muscle wasting by preserving mitochondrial function and restoring lipid metabolic capacity. (A) Representative TEM images of skeletal muscles from rats in the shNC+sham, shD3+sham, shNC+CLP and shD3+CLP groups (scale bar: 1 μm), with quantification of mitochondrial damage (mitochondrial injury criteria were listed in the Methods section; n = 8). (B) To assess mitochondrial function, oxygen consumption rate (OCR) of C2C12 myoblasts transfected with shNC or shDio3 ± 100 μg/mL LPS was measured using a seahorse XFe96 analyzer. (C) Representative red oil staining images of TA muscles from rats under the conditions described in (A, n = 6) (scale bar, 50 μm). (D) Quantitative RT-PCR analysis of lipid metabolism genes, including *CD36*, *CPT1b*, *LCAD*, *MCAD*, and *SCAD*, in TA muscles of rats, with experimental groups corresponding to those in (A, n = 6). (E) Sample trace of respiration in isolated TA muscle mitochondria of each group offered palmitoyl CoA and carnitine with malate as respiratory substrates all ± 3 mM etomoxir (Biological replicates n = 3, technical replicates n = 4). (F) Calculation of ADP driven and FCCP-stimulated respiration which is dependent on CPT1b (ΔOCR = non-etomoxir treated OCR minus etomoxir treated OCR). (G) Representative immunofluorescence images of BIDOPY (green) and Mitotracker (red) in C2C12 myoblasts transfected with either sh-vector (shNC) or shDio3 constructs treated with 100 μg/mL LPS (scale bars, 20 and 50 μm, respectively; n = 6), with quantification provided. (H) Representative immunofluorescence staining images of MYH7 and MYH4 in TA muscles of rats (scale bar, 100 μm). (I) Quantification of (H, n = 6). (J) Quantification of muscle fiber diameters from HE staining of TA muscles from each group. (K) TA muscle-to-body weight ratio (n = 6). (L) qRT-PCR analysis of myogenesis-related genes (*MyoG*, *MyoD*) in TA muscles (groups as in A; n = 3). (M) Immunoblots of anabolic markers (mTOR, *p*-mTOR, AKT, *p*-AKT) in TA muscles (groups as in A; n = 3). (N) Immunoblots of catabolic markers (FOXO1, *p*-FOXO1, MuRF1, ATROGIN1) in TA muscles (groups as in A; n = 3). To ensure blot comparability, identical sample volumes were loaded for both phospho- and total-protein detection, with all membranes probed for β-tubulin as loading control. Data are mean ± SD. *, $P < 0.05$; NS, not significant. A, B, C, D, J, K, L, M and N: One-way ANOVA or Kruskal-Wallis test with Tukey's post hoc; G and I: Two-tailed unpaired *t*-test.

expression in vitro, with an even greater increase observed following LPS exposure (Fig. 4C and S4B). Further analyses revealed that PINK1 and Parkin's levels were significantly higher in total cell extracts after Dio3 knockdown, with a decrease in cytoplasmic levels but a significant increase in mitochondrial levels (Fig. 4D, E and 4F). To validate whether Dio3 knockdown facilitates mitophagy primarily through the PINK1/Parkin pathway, we interfered with PINK1 expression (Fig. 4G). This interference significantly attenuated the increase in mitophagy (Fig. 4H) and the preservation of mitochondrial function initially observed by knockdown of Dio3 (Fig. 4I–S4C and S4D). Furthermore, the beneficial impact of Dio3 knockdown on anabolic metabolism was substantially diminished after interfering with PINK1 expression (Fig. 4J). Thus, these results demonstrate that the mitophagy-enhancing and metabolism-improving effects of Dio3 knockdown are dependent on the PINK1/Parkin pathway.

2.5. Depletion of NAD facilitates PINK1 acetylation and its degradation

To explore the regulatory mechanism of PINK1 induced by Dio3 knockdown, C2C12 cells were treated with gradient concentrations of T3, with or without LPS exposure. We observed that in the absence of LPS, only 5 nM T3 significantly increased PINK1 expression. However, with LPS treatment, PINK1 expression increased as T3 concentrations rose (Fig. 5A). To examine whether T3 affects *PINK1* transcriptionally, C2C12 cells were treated with 2 nM T3. This treatment enhanced TH responsiveness but did not induce *PINK1* expression (Fig. S5A). Additional experiments with various T3 concentrations also showed no significant transcriptional induction of *PINK1* (Fig. 5B). Given that PINK1 activation depends on MMP [31], Mitotracker staining indicated that the shD3+LPS group had a significantly higher MMP compared to the shNC+LPS group (Fig. 5C and S5B). These results suggest that under septic conditions, the regulation of PINK1 by the TH axis may involve post-translational modifications.

Given the significant influence of TH on tissue metabolism, we performed metabolomics analysis on muscle samples of septic rats. This analysis revealed 23 differential metabolites across the groups: shNC+sham, shNC+CLP, and shD3+CLP (Fig. 5D). Upon intersecting the differential metabolites between the shNC+CLP and shD3+CLP groups, we identified 4 distinct metabolites (Fig. 5E). Levels of L-methionine and nicotinamide riboside (NR) were elevated, while Oleamide and 2-methoxy estradiol (2-ME2) were reduced (Fig. 5F). Among the four metabolites mentioned, NR, as a precursor of the nicotinamide adenine dinucleotide (NAD) salvage synthesis pathway, has garnered our attention (Fig. 5G). Since impaired NR utilization can lead to tissue NAD depletion, adversely affecting the deacetylating activity of sirtuins [32]. Accordingly, we measured tissue levels of NAD and its reduced form, NADH, following CLP modelling, and observed a significant reduction in both metabolites and the NAD/NADH ratio. Interestingly, these levels and the ratio were significantly restored after Dio3 knockdown (Fig. 5H). Western Blot analysis confirmed a notable increase in protein acetylation levels after CLP, which was reversed by Dio3 knockdown (Fig. 5I and S5C). Additionally, significantly elevated expression of SIRT1 and SIRT3 was also observed following Dio3 knockdown, which may contribute to improved NAD metabolism (Fig. S5D). Furthermore, Dio3 knockdown significantly preserved mitochondrial SIRT3 expression following LPS stimulation, demonstrating its role in regulating protein deacetylation (Fig. S5E and S5F).

Prior studies have shown that PINK1 and Parkin are subject to acetylation modification [33]. We thus investigated whether Dio3 knockdown could enhance PINK1 and Parkin expression by altering NAD metabolism. C2C12 cell treatment with 3-TYP, an inhibitor of Sirtuin deacetylases, and LPS increased the acetylation of PINK1 and Parkin, whereas NAD supplementation decreased it (Fig. 5J–S5E and S5F). Moreover, treatment with the proteasome inhibitor MG132 indicated that acetylation promotes PINK1 degradation (Fig. 5K). Since PINK1 is primarily modified by cleavage via the enzymes Presenilin Associated Rhomboid Like (PARL) and OMA1 Zinc Metallopeptidase (OMA1) [34,35], we performed Co-IP assays for PARL and OMA1. The findings revealed that neither 3-TYP nor LPS treatment, individually or in combination, exerted a significant influence on the binding affinity of PARL to PINK1 (Fig. 5L and S5G). However, a notable enhancement in the binding of OMA1 was observed (Fig. 5M and S5H), implying that elevated acetylation levels may facilitate this interaction, potentially impacting PINK1's stability.

2.6. Dio3 knockdown alleviates NAD depletion via NRK2 induction

Nicotinamide riboside kinase (NRK), the rate-limiting enzyme in the NAD salvage synthesis process, exhibits distinct regulatory patterns (Fig. 6A) [36]. Our findings reveal that the transcriptional expression of both *NRK1* and *NRK2* was significantly decreased following CLP modelling (Fig. 6B). Given that NRK2 is specifically expressed in skeletal muscle and exhibits higher expression levels than NRK1, we focused on the modulation of NRK2 [32]. CLP modelling significantly suppressed NRK2 expression (Fig. 6C), which was substantially alleviated by Dio3 knockdown both at protein and mRNA level (Fig. 6D and S6A). Similarly, LPS treatment significantly reduced NRK2 expression in C2C12 cells, an effect that was effectively reversed by Dio3 knockdown, particularly at the transcriptional level (Fig. 6E–F). Utilizing the JASPAR database, we identified high-affinity binding sites for THRα and its heterodimeric partners Retinoid X Receptor Alpha (RXRα) and Retinoid X Receptor Gamma (RXRγ) on the NRK2 promoter, with THRα achieving the highest score (Table S3). ChIP-PCR and RT-qPCR results confirmed the binding of THRα to the NRK2 promoter, exerting positive transcriptional regulation (Fig. 6G and H, and S6B). To assess whether Dio3 knockdown enhances tissue NAD metabolism via increased NRK2 expression, we modulated NRK2 levels (Fig. S6C) and monitored intracellular NAD and NADH. Interference with NRK2 expression

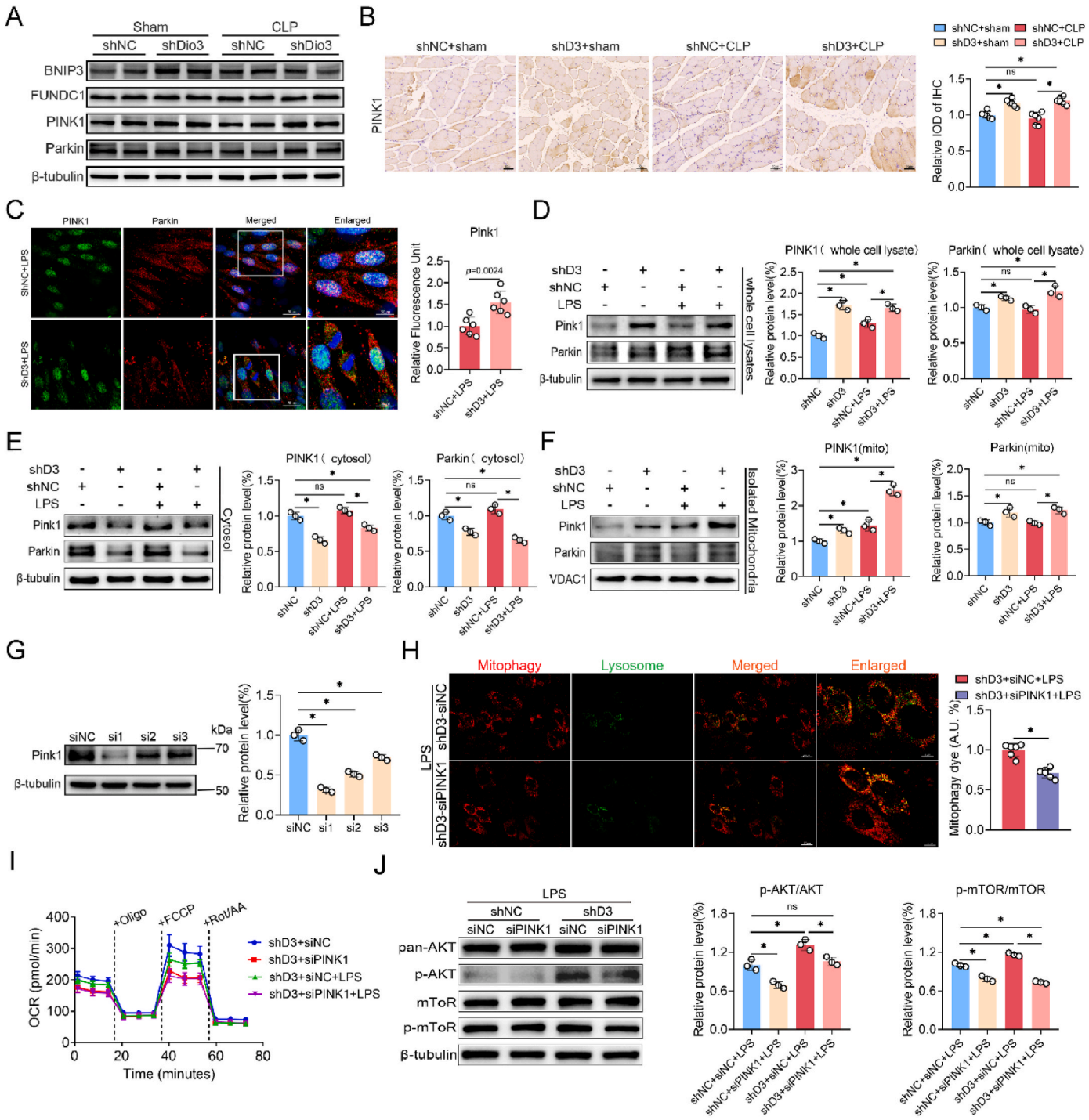

Fig. 4. Dio3 Knockdown promotes mitophagy and anabolism in a PINK1/Parkin-Dependent Manner. (A) Representative immunoblots of mitophagy-associated proteins (BNIP3, FUNDC1, PINK1, Parkin) in TA muscles from shNC+sham, shD3+sham, shNC+CLP, and shD3+CLP groups. (B) IHC staining of PINK1 in TA muscles (groups as in A; scale bar: 50 μm; n = 6), with quantification. (C) IF images of PINK1 (green) and Parkin (red) in shNC- or shDio3-transfected C2C12 myoblasts treated with 100 μg/ml LPS (scale bars: 20 μm, 50 μm; n = 6), with quantification. (D) Immunoblots of PINK1 and Parkin in C2C12 myoblasts transfected with shNC or shDio3 treated with or without 100 μg/ml LPS at whole-cell level. (E) Immunoblots of PINK1 and Parkin (groups as in D) at cytosolic level. (F) Immunoblots of PINK1 and Parkin (groups as in D) at mitochondrial level. (G) Immunoblots of PINK1 in C2C12 myoblasts transfected with PINK1-targeting siRNAs. (H) Mitophagy assessment in shD3 myoblasts transfected with siPINK1 or siNC. Representative images show Mitophagy dye (red) and Lyso dye (green), with merged/enlarged views (scale bars: 20 μm, 8 μm; n = 6). (I) Oxygen consumption rate (OCR) of shD3 myoblasts transfected with siPINK1 or siNC treated with or without 100 μg/mL LPS was measured using a seahorse XFe96 analyzer. (J) Immunoblots of anabolic markers (mTOR, *p*-mTOR, AKT, *p*-AKT) in C2C12 myoblasts (groups as in D), with quantification. To ensure blot comparability, identical sample volumes were loaded for both phospho- and total-protein detection, with all membranes probed for β-tubulin as loading control. Data are mean ± SD. *, $P < 0.05$; NS, not significant. B, D, E, F, G, and J: One-way ANOVA with Tukey's post hoc; C and H: Two-tailed unpaired *t*-test.

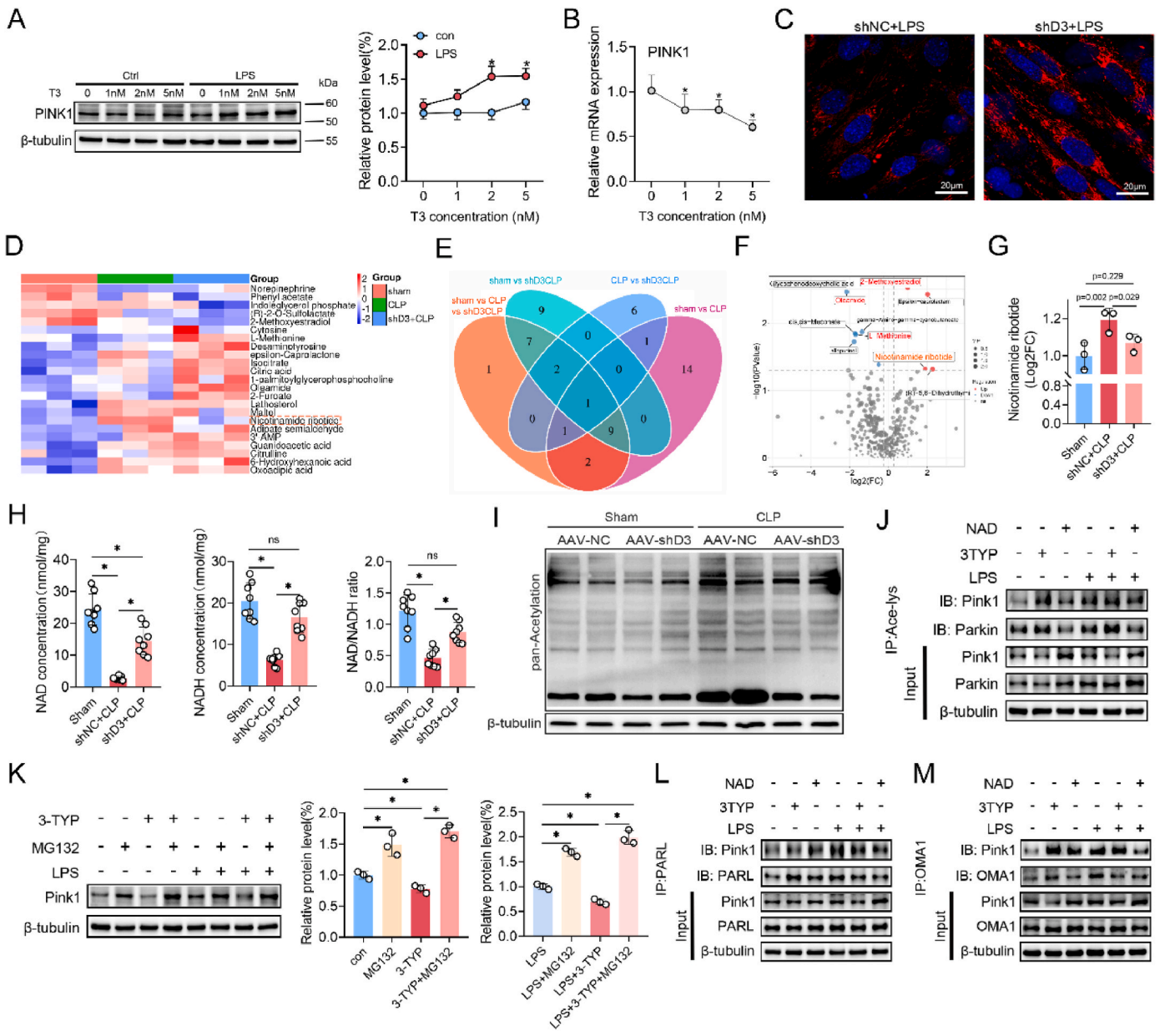

Fig. 5. NAD Depletion Promotes PINK1 Acetylation and Degradation. (A) Immunoblots of PINK1 expression in C2C12 cells treated with T3 (0, 1, 2, 5 nM) for 24 h ± LPS (100 μg/mL), with quantification (n = 3). (B) qRT-PCR analysis of *PINK1* mRNA levels in C2C12 cells exposed to T3 (1, 2, 5 nM) for 24 h (n = 3). (C) Representative Mitotracker staining in shNC+LPS andshD3+LPS cells (scale bar: 20 μm; n = 6). (D) Cluster analysis of differential metabolites in TA muscles from shNC+sham, shNC+CLP, and shD3+CLP groups (n = 3). (E) Venn diagram of distinct metabolite subsets across groups (n = 3). (F) Volcano plot of differential metabolites in TA muscles of shNC+CLP vs. shD3+CLP rats (n = 3). (G) Nicotinamide riboside levels in TA muscles (groups as in D), quantified from metabolomic data (n = 3). (H) NAD/NADH content in TA muscles (groups as in D; n = 8). (I) Immunoblots of pan-acetylation in TA muscles from shNC+sham, shD3+sham, shNC+CLP, and shD3+CLP groups (n = 3). (J) Immunoprecipitation (IP) with anti-pan-acetylation antibody in C2C12 cells treated with 3-TYP (10 μM), NAD (5 mM), or LPS (100 μg/ml). Input: 20 % lysate. (K) Immunoblots of C2C12 cells treated with 3-TYP, MG132, or LPS, with quantification (n = 3). (L) IP with anti-PARL antibody in C2C12 cells (groups as in J). Input: 20 % lysate. (M) IP with anti-OMA1 antibody in C2C12 cells (groups as in J). Input: 20 % lysate. Data are mean ± SD. A, B: Two-tailed unpaired *t*-test; G, H, K: One-way ANOVA with Tukey's post hoc. *, $P < 0.05$; NS, not significant.

significantly compromised the protective effect of Dio3 knockdown on NAD metabolism (Fig. 6I). It also led to a noticeable reduction in the Dio3-induced upregulation of PINK1 and Parkin (Fig. 6J and S6D) and a decline in mitophagy levels (Fig. 6K). Furthermore, NRK2 interference significantly abolished the protective effects of Dio3 knockdown on mitochondrial function (Fig. 6L and S6E).

In conclusion, Dio3 knockdown facilitates THRα binding to the NRK2 promoter, thereby restoring NAD salvage synthesis and ensuring tissue NAD homeostasis through NRK2 induction.

3. Discussion

Although extensive research has evaluated the impact of TH on mitochondrial function, investigations into their role under stress conditions, particularly regarding mitophagy, remain limited. Our study reveals a significant decrease in TH activity in skeletal muscle during early sepsis. By specifically knocking down Dio3 in skeletal muscle, we effectively restored local TH activity, which resulted in increased mitophagy and alleviation of the metabolic disruptions caused by sepsis. Mechanistically, Dio3 knockdown restored the expression of THRα,

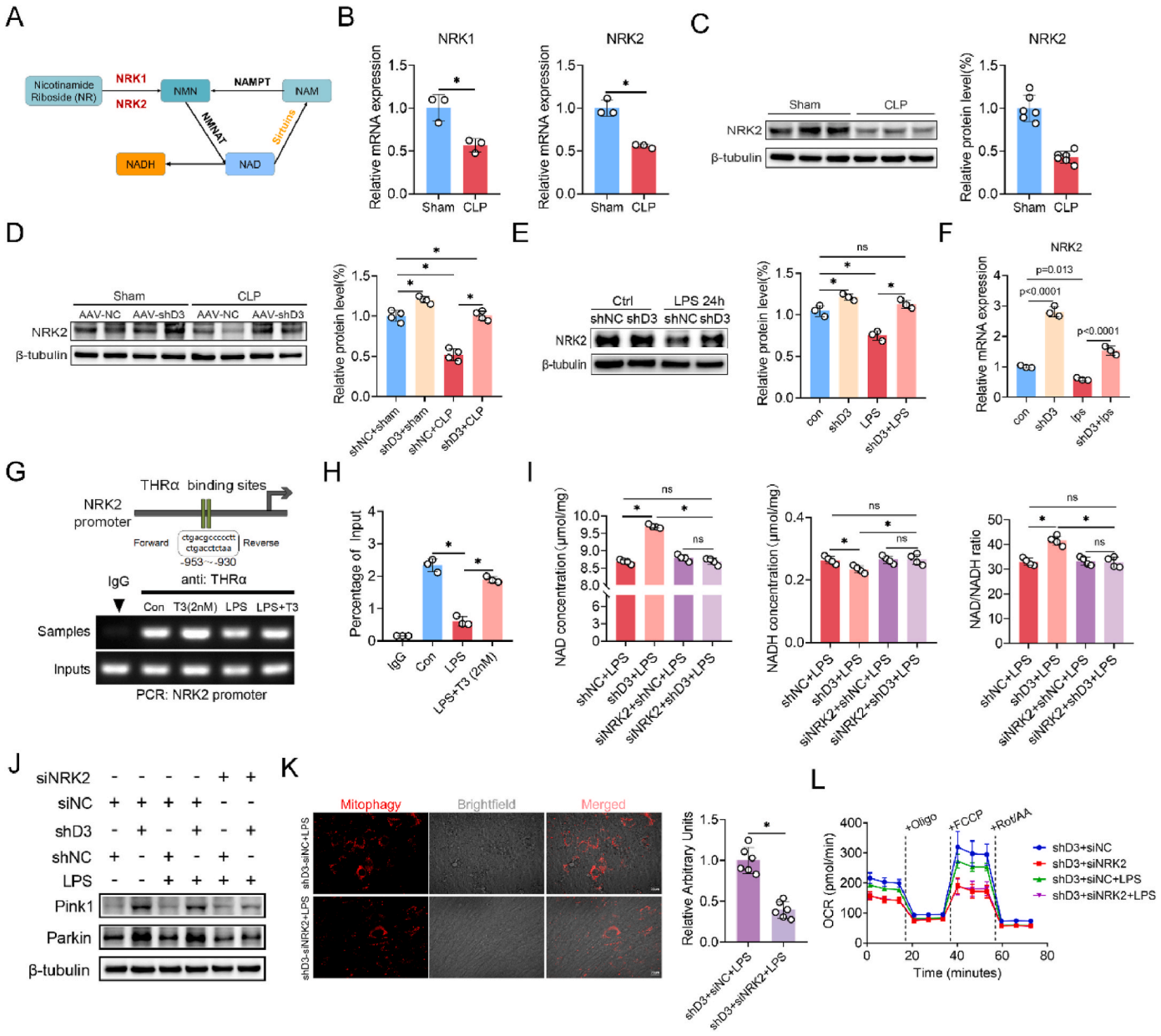

Fig. 6. Dio3 Knockdown Ameliorates NAD Depletion through NRK2 Induction. (A) Schematic of the NAD salvage synthesis pathway. (B) qRT-PCR analysis of *NRK1* and *NRK2* mRNA levels in TA muscles from sham or 48h-CLP rats (n = 3). (C) Immunoblots of NRK2 in TA muscles from sham or 48h-CLP groups, with quantification (n = 6). (D) Immunoblots of NRK2 in TA muscles from shNC+sham, shD3+sham, shNC+CLP, and shD3+CLP groups, with quantification (n = 6). (E) NRK2 expression in C2C12 myoblasts transfected with shNC or shD3 lentivirus and treated with PBS or LPS (immunoblots with quantification; n = 3). (F) qRT-PCR analysis of *NRK2* mRNA levels in cells treated as in (E, n = 3). (G) Agarose gel electrophoresis of PCR-amplified DNA from THRα immunoprecipitates in C2C12 cells treated with PBS, T3 (2 nM), LPS, or LPS+T3 (2 nM). (H) qRT-PCR quantification of DNA samples from (G, n = 3). (I) NAD, NADH levels in C2C12 cells transfected with shNC, shD3, and co-transfected with siRNA-NC, or siRNA-NRK2, followed by LPS (100 μg/mL) treatment (n = 4). (J) Immunoblots of PINK1 and Parkin in C2C12 cells transfected as in (I) and treated with PBS or LPS (n = 3). (K) Mitophagy assessment in C2C12 cells transfected with lenti-shD3, siRNA-NC, or siRNA-NRK2, exposed to LPS (scale bar: 20 μm; n = 6). (L) Oxygen consumption rate (OCR) of shD3 myoblasts transfected with siNRK2 or siNC treated with or without 100 μg/mL LPS was measured using a seahorse XFe96 analyzer. Data are mean ± SD. *, $P < 0.05$; NS, not significant. B, C, K: Two-tailed unpaired *t*-test; D, E, F, H, I: One-way ANOVA with Tukey's post hoc.

facilitated its binding to the NRK2 promoter, counteracted its suppression induced by sepsis, and revitalized the NAD salvage synthesis, thereby improving NAD metabolism in skeletal muscle. The improved NAD metabolism subsequently promoted the decrease in the acetylation levels of PINK1, impeding its cleavage mediated by OMA1 and subsequent degradation, thus promoting mitophagy. In summary, our research bridges a knowledge gap concerning the modulation of mitophagy by the TH axis under stress, identifies diminished TH activity as a pivotal factor limiting mitophagy in stressed skeletal muscles, and implicates it as a major contributor to sepsis-induced metabolic disarray and muscle wasting. Targeted inhibition of Dio3 in skeletal muscle may offer a novel therapeutic approach to combat muscle wasting.

Among the various organ dysfunctions sepsis induces, muscle wasting is notably prevalent yet often overlooked [37]. Acute stress including sepsis triggers accelerated catabolism in skeletal muscle, supplying the liver with essential amino acids for gluconeogenesis [38]. In this process, skeletal muscle is sacrificially utilized as an energy source for critical organs, akin to wartime resource allocation where

reserves are continuously directed to the frontline. However, this strategy, despite initial survival, results in resource depletion and damage that may require extensive recovery or even lead to collapse. Clinically, this is reflected in the various organ dysfunctions, including diaphragm weakness, respiratory muscle fatigue and muscle atrophy, and persistently high long-term mortality rates among sepsis survivors [2]. Noteworthy, many sepsis survivors enter a state of persistent inflammation, immunosuppression, and catabolism syndrome (PIICS), with a mortality peak around two years post-discharge [39]. Among the myriad symptoms of PIICS, muscle wasting, a key indicator of sustained catabolism, extends from the acute phase of sepsis through the PIICS state and even to death [40]. Moreover, patients with sepsis complicated by sarcopenia experience an 8.3-fold increase in one-year mortality rate compared to those without sarcopenia, a risk that significantly exceeds the mortality impact of age-related sarcopenia [41]. Despite decades of research and the clinical implementation of therapeutic strategies such as early mobilization, nutritional support, and neuromuscular electrical stimulation, their effectiveness in reversing muscle atrophy is still limited [40]. For instance, clinical nutritionists have historically advocated for early and adequate nutritional support to combat muscle wasting [42]. Yet, recent clinical studies indicate that such an approach may be detrimental, as increased nutritional supplementation fails to compensate for the loss of skeletal muscle mass effectively. In response to these findings, clinical nutritionists have reconsidered their strategies, suggesting that a higher protein intake could significantly improve muscle wasting [43]. Although this approach has been recommended by nutritional societies, recent studies have demonstrated its ineffectiveness [5]. These strategies have neglected the critical issue of anabolic resistance, leading to a mismatch between nutritional provision and utilization and imposing additional burdens on organs. Therefore, restoring anabolic responsiveness is essential for reversing muscle wasting. Our findings demonstrate that restoring local TH activity through Dio3 knockdown ameliorates sepsis-induced skeletal muscle lipid metabolic dysfunction, mitigates sepsis-induced fast-to-slow myofiber conversion and reinstates the activation of the AKT-mTOR pathway which plays a central role in anabolic processes, thereby ameliorating anabolic resistance effectively. Another question should be mentioned is that though exogenous T3 or T4 supplementation is more accessible, clinical evidence suggests that these strategies are regarded as not beneficial or even detrimental in sepsis, thus not advocated in clinical settings [44]. Therefore, tissue-specific Dio3 inhibition emerges as a superior alternative in boosting local TH activity. More importantly, unlike exogenous T3 supplementation, this approach restores tissue TH activity without disrupting the feedback regulation of the TH axis. Furthermore, under physiological conditions, skeletal muscle TH activity is primarily regulated by Dio 2, while Dio3 expression is minimal [13]. Thus, Dio3 knockdown is unlikely to shift local TH status from suppression to a toxic hyperthyroid state. This conclusion is further supported by our measurements of local TH receptor and transporter expression in Dio3 knockdown tissues. As targeted drug delivery systems and small molecule inhibitors continue to evolve, forthcoming medications aimed at Dio3 could present novel therapeutic strategies for the clinical management of sepsis-induced muscle wasting.

Numerous investigations have proven that mitochondrial function plays a pivotal role in maintaining metabolic homeostasis. Meanwhile, TH is well-established as a key regulator in MQC. Thus, to delineate the mechanisms by which TH mitigates sepsis-induced metabolic disturbances in muscle, we concentrate on mitochondrial function. Emerging evidence shows that TH safeguards mitochondria and organ function by promoting mitophagy across various tissues. Specifically, in studies on subarachnoid hemorrhage, exogenous T3 supplementation has been demonstrated to boost mitophagy through the PINK1/Parkin pathway, thus mitigating neuronal damage [45]. Similarly, T3 supplementation has been observed to protect the myocardium by enhancing mitophagy in a murine model of myocardial ischemia-reperfusion injury [46]. Our study corroborates these findings, revealing a strong correlation between local TH activity and the expression levels of proteins involved in mitophagy. Furthermore, the high correlation between Dio3 expression and the levels of BNIP3 and PINK1 implies a positive association between local TH activity and the extent of mitophagy. To validate these observations, we specifically knocked down Dio3 expression both in vivo and in vitro, confirming that Dio3 inhibition significantly enhances mitophagy and preserves mitochondrial function in a PINK1/Parkin-dependent manner.

Under stress conditions, PINK1 accumulates on the OMM in response to decreased MMP, thereby initiating mitophagy. Interestingly, inhibition of Dio3 protects mitochondrial function, resulting in preserved MMP. While genes such as NF-KB, FOXO3, and NRF1 are known to transcriptionally regulate PINK1 expression [21], our in vivo and in vitro experiments did not reveal an increase in PINK1 mRNA levels, suggesting the involvement of post-translational modifications. Metabolomic analysis revealed an accumulation of L-Methionine in skeletal muscle following CLP modelling, indicating a potential utilization deficit. L-methionine, a precursor to glutathione, is essential for antioxidant defenses, and its increased levels may suggest a reduced antioxidant capacity. Additionally, L-Methionine's conversion to S-adenosylmethionine, a key methyl donor in DNA methylation, is another critical function [47]. Research indicates that downregulation of Methionine metabolism in macrophages affects PP2Ac methylation, influencing PINK1 expression [48]. However, gene methylation modifications typically impact gene expression at the transcriptional level, which is inconsistent with our findings. Oleamide, a byproduct of lipid metabolism, exerts anti-inflammatory and antioxidant effects in skeletal muscle but is not established as a direct participant in post-translational modifications [49]. Similarly, 2-ME2, which plays broad roles in skeletal muscle, mitigates tissue inflammation by inhibiting inflammatory cytokines such as TNFα and IL-6 and promotes muscle growth by regulating cell cycle proteins, yet there is no evidence of its involvement in protein post-translational modifications [50,51]. Lastly, we observed the accumulation of NR in tissues. NR, a precursor of NAD, is vital for maintaining tissue NAD levels through the salvage synthesis pathway. Exogenous NR supplementation contributes to various physiological activities in skeletal muscle, including anti-inflammatory effects, enhancement of endurance and strength, metabolic improvement, and MQC [52–54]. Importantly, NR enhances the deacetylase activity of Sirtuins through the promotion of NAD metabolism [55].

Research by Shen Weili et al. has demonstrated that the absence of SIRT3 leads to excessive acetylation of PINK1, thereby inhibiting mitophagy in cardiomyocytes [56]. Additionally, enhancing SIRT1 activity has been shown to ameliorate sodium arsenite-induced acute kidney injury by upregulating the expression of PINK1 [57]. Collectively, these studies suggest that the acetylation status of PINK1 impedes its expression. Our findings also indicate a significant increase in acetylated-PINK1 levels under inflammatory conditions. However, the specific mechanism by which acetylation affects PINK1 expression remains elusive. Under physiological conditions, PINK1 is modified by IMM proteases, and inhibiting its cleavage favors PINK1 stabilization. PHB2 has been identified to upregulate PINK1 expression by inhibiting PARL [58], while TIM23 enhances PINK1 stability by preventing the interaction between OMA1 and PINK1 [59]. Although both PARL and OMA1 facilitate PINK1 degradation through cleavage, they operate in distinct biological contexts—with PARL predominantly active under physiological conditions and OMA1 primarily implicated under stress [34,59]. Our data indicate that LPS and 3-TYP treatment enhances the binding of PINK1 to OMA1, an effect that is reversed by NAD treatment. This suggests that PINK1 acetylation promotes its degradation through OMA1-mediated cleavage. Thus, our study has identified the mechanism underlying TH axis-induced mitophagy in skeletal muscle and clarified how the TH axis regulates PINK1, thereby establishing a novel regulatory pattern for future research.

Previous studies have demonstrated a significant decline in Sirtuins activity across multiple tissues during sepsis. This suppression of sirtuins

may be attributed to inflammatory responses and ROS accumulation, which can impair sirtuins function through transcriptional repression or interference with NAD + metabolism [60]. Notably, THs also serve as a crucial regulator of sirtuins activity. Emerging evidence indicates that T3 can enhance SIRT3 transcription by upregulating PGC-1α expression, while simultaneously promoting SIRT1 expression through AMPK pathway activation [61,62]. These findings suggest that Dio3-mediated local TH inactivation in inflammatory microenvironments may represent an additional mechanism contributing to sirtuins dysfunction. In the present study, we observed that skeletal muscle exhibits profound NAD + metabolic disturbances during the early stages of sepsis. Importantly, Dio3 knockdown was found to ameliorate these NAD + metabolic abnormalities, thereby establishing a biochemical foundation for subsequent sirtuins activation.

Growing evidence demonstrates that correcting NAD + metabolic disturbance exerts organ-protective effects during sepsis [63]. As NAD cannot be directly absorbed through exogenous supplementation, the focus has shifted to its precursors, nicotinamide mononucleotide (NMN) and NR. Despite ongoing debates about the supplementation strategies for NMN and NR, their ability to enhance NAD levels in skeletal muscle is well-documented [64,65]. In the realm of sepsis research, NR has attracted considerable interest. It has been demonstrated to alleviate T cell exhaustion in septic mice, effectively reversing sepsis-induced immunosuppression [66]. Moreover, NR supplementation has been reported to improve survival rates and mitigate lung and heart injuries in CLP mouse models [67]. Notably, the physiological effects of NR are dependent on NRKs. Interestingly, our findings revealed decreased expression of both NRK1 and NRK2 in skeletal muscle following CLP modelling, implying an impairment of the NAD salvage synthesis. Furthermore, the efficacy of exogenous NR supplementation exerting on skeletal muscle may be compromised under such conditions. Our findings reveal that THRα, acting as a transcription factor, regulates the expression of NRK2, thereby directly modulating NAD metabolism through the enhancement of NAD salvage synthesis. This discovery fills a knowledge gap in our understanding of the direct regulation of NAD metabolism by the TH axis. In summary, these findings provide novel insights into the metabolic shifts within the NR/NAD axis in skeletal muscle during sepsis.

Our study has several limitations. Initially, we utilized samples from patients in the recovery phase as controls instead of samples from healthy individuals, owing to the practical and ethical constraints of obtaining biopsies from healthy subjects. Although muscle samples from recovering patients can approximate the characteristics of healthy muscle to an extent, inherent biases cannot be entirely ruled out. Additionally, a murine model with targeted skeletal muscle Dio3 ablation could provide more compelling evidence than localized AAV administration; however, systemic Dio3 ablation might induce developmental abnormalities in muscle tissues [68]. Another issue that needs to be addressed is that the current evidence supporting the improvement of skeletal muscle lipid metabolism by Dio3 knockdown remains largely indirect, lacking direct experimental validation such as enzyme activity assays or C14 tracer studies. Finally, although accumulating evidence suggests that SIRT3 predominantly mediates PINK1 deacetylation under stress conditions, our study did not definitively establish a direct interaction between SIRT3 and PINK1, which remains an area for further investigation.

In summary, our study demonstrates that restoring local TH activity in sepsis enhances mitophagy in skeletal muscle, thereby alleviating the associated metabolic dysregulation. Our research also reveals a novel mechanism by which increased NRK2 expression, achieved through Dio3 inhibition, improves tissue NAD metabolism and reduces PINK1 acetylation levels, thereby preserving its stability against OMA1-mediated degradation. These insights offer new avenues and potential targets for treating sepsis-induced muscle wasting.

4. Materials and methods

4.1. Human skeletal muscle samples collection

Ten severely ill patients (range 33–71 years; n = 5 male, n = 5 female) admitted to the Intensive Care Unit (ICU) at Nanjing Drum Tower Hospital were enrolled in this study. Senior specialists performed skeletal muscle biopsies on these patients under ultrasound guidance. The obtained samples were collected for subsequent immunohistochemistry (IHC) analyses. Informed consent was obtained in writing from all participants, and the procedure was conducted in accordance with the ethical standards set by the Nanjing Drum Tower Hospital's ethics committee (Ethics number: 2023-427-03).

4.2. Animal experiments design

Male Sprague Dawley rats, aged 8 weeks (n = 12) and 4 weeks (n = 24), were obtained from Charles River Company (Nanjing, China). The animals were housed in a pathogen-free environment with a 12-h light/dark cycle at a temperature of 24 °C. They had free access to water and food. Sepsis was induced using the CLP method, as previously described. Local administration of pAAV-EGFP-U6-shDio3 (1 x 10^{11} genomic copies per rat, OBiO Technology, Shanghai, China) was used to specifically knock down Dio3 expression in the TA muscle, utilizing the shDio3 sequence: GCGCGACGTTGACTTCCTTAT. The experimental design was divided into two parts: in the first part, animals were divided into a sham group (n = 6) and a 24-h CLP group (n = 6); in the second part, there were four groups: a shNC+sham group (n = 6), a shDio3 (shD3)+sham group (n = 6), a shNC+CLP group (n = 6), and a shD3+CLP group (n = 6). Rats received either AAV-shDio3 for Dio3 knockdown or AAV-vector as a negative control. Twenty-four hours post-CLP surgery, with a 48-h duration for the second part of the study, the rats were euthanized, and tissue samples were collected via a surgical procedure. A portion of the collected tissues was fixed in 4 % paraformaldehyde, while the remainder was stored at −80 °C for subsequent molecular analysis. All animal procedures were conducted in accordance with the ARRIVE guidelines and were approved by the Ethics Committee of Nanjing Drum Tower Hospital (Ethics number: 2022AE02004).

4.3. Cell culture and treatments

The C2C12 murine myoblast cell line (Pricella Biotechnology, Wuhan, China), was cultivated in an environment enriched with Dulbecco's Modified Eagle Medium (DMEM, Gibco, USA), which was further supplemented with 10 % fetal bovine serum (FBS, Hyclone, USA) and a mixture of 1 % penicillin-streptomycin (Gibco, USA). The cells were maintained in a climate of 5 % CO2 in equilibrium with air, within a consistently regulated temperature of 37 °C, and a humidified setting. The process of cell differentiation adhered to established methodologies. To simulate inflammatory conditions in vitro, the culture medium was supplemented with 100ug/mL lipopolysaccharide (LPS). In accordance with the experimental protocol, a range of compounds was applied, such as Bafilomycin A1 (HY-100558, MCE, USA), Liothyronine (HY-A0070A, MCE, USA), 3-TYP (HY-108331, MCE, USA), NAD (N7004, Sigma-Aldrich, USA), and MG-132 (HY-13259, MCE, USA).

4.4. Lenti-virus and siRNA transfection

C2C12 were seeded in a six-well plate one day prior transfection. When the confluency reached 30–50 %, culture medium was replaced and adequate content of lenti virus containing shDio3 (sequence used for lenti-virus construction: CAGCGCAGCGAGAGTACTA) was added (MOI: 100). Polybrene was used for enhancing the efficacy of transfection. 48h post transfection, cells were collected and transferred to 6 cm culture dishes, and puromycin was used for purification. siRNA transfection was

performed using a commercial transfection reagent (GenMute, signagen, USA) following the manufacturer's instructions with the final concentration of siRNA to be 40 nM. The siRNAs were constructed and purchased from OBiO Technology (Shanghai, China). The sequences used for siPINK1 is Forward: CACUGUUCCUCGUUAUGAAGATT, Reverse UCUUCAUAACGAGGAACAGUGTT, and siNRK2 is Forward: GAAUGCAAGCGGAGGAGAATT, Reverse UUCUCCUCCGCUUGCAUUCTT.

4.5. Mitophagy detection

The C2C12 myoblasts were initially seeded in customized confocal culture dishes in preparation for subsequent experimental manipulations. Following the outlined experimental protocols, the cells underwent differentiation and treatment processes. For the assessment of mitophagy in living cells, the Mitophagy Detection Kit (MD01, Donjindo, Japan) was utilized, strictly adhering to the guidelines provided by the manufacturer. The ensuing fluorescent images were then captured using a laser-scanning confocal microscope (FV3000, Olympus Corporation, Japan).

4.6. Mitochondrial isolation

Rat TA muscle mitochondria were isolated according to standard techniques with slightly modifications [69]. Briefly, the TA muscle was minced and rinsed several times in MSHE [70 mM sucrose, 210 mM mannitol, 5 mM HEPES (pH 7.2), and 1 mM EGTA with 0.5 % (w/v) fatty acid-free BSA] to remove blood. Tissue was disrupted using a glass Dounce homogenizer (between 20 and 40 strokes). The homogenate was centrifuged at 1000g for 10 min and the supernatant was centrifuged at 11000g for 10 min. The light layer from the pellet was removed and the remaining pellet was resuspended in MSHE, centrifuged at 8000g for 10 min, and resuspended in a minimal volume of MSHE.

4.7. Seahorse analysis

Mitochondria stress test for cells: Cells were seeded in an XF96 microplate (Seahorse Bioscience) at a density of 8000 cells per well and allowed to differentiate for 48 h. Mitochondrial respiration was assessed using the XF96 Extracellular Flux Analyzer (Seahorse Bioscience) following the manufacturer's protocol. To evaluate key parameters of mitochondrial function, sequential injections of mitochondrial modulators were performed: (1) 15 μM oligomycin (ATP synthase inhibitor) to measure uncoupled respiration (proton leak); (2) 10 μM FCCP (mitochondrial uncoupler) to induce maximal respiratory capacity; and (3) 5 μM rotenone/antimycin A to determine non-mitochondrial oxygen consumption.

Substrate oxidation stress test for isolated mitochondria: This part of experiments rigorously adhered to established methodological protocols from prior research [70]. Briefly, phosphorylating respiration was measured in isolated TA muscle mitochondria (5 μg/well), and offered 40 μM palmitoyl CoA, 0.5 mM malate, 0.5 mM carnitine and 4 mM ADP. Uncoupler stimulated respiration was measured after addition of oligomycin (2.25 μM) and FCCP (1.5 μM). All rates were corrected for background by subtracting the oxygen consumption rate insensensitive to 0.2 μM rotenone and 1 μM antimycin A. Etomoxir (3 μM) was acutely added to the experimental medium 15 min prior to taking initial measurements.

4.8. NAD/NADH detection

NAD and NADH levels were quantified in muscle tissue samples and cellular lysates using the NAD/NADH Assay Kit (S0176S, Beyotime, China), in strict accordance with the manufacturer's protocol.

4.9. HE staining

Rat skeletal muscle paraffin sections were stained with hematoxylin and eosin to assess pathological structural changes. The resulting images were acquired using a Digital Pathology System (3D-Histech, Pannoramic MIDI, Hungary).

4.10. Transmission electron microscopy (TEM)

For TEM analysis of tissues, rat skeletal muscle specimens were initially fixed in a 2.5 % glutaraldehyde solution. Subsequent post-fixation was performed using 3 % osmium tetroxide (OsO4) for a duration of 2 h. The specimens underwent a dehydration process through a serial gradient of ethanol concentrations, followed by embedding in Epon resin. Ultrathin sections, 100 nm in thickness, were prepared and examined using a transmission electron microscope operated at an acceleration voltage of 80 kV (Hitachi H7500 TEM, Japan).

4.11. Electron microscopy parameters for assessing mitochondrial impairment

Disruption of membrane integrity: A distinct gap $\geq$10 nm between two segments of the outer mitochondrial membrane (with no membranous connection). Destruction or disorganization of cristae: Loss of continuity in the inner mitochondrial cristae with gaps $\geq$20 nm, or fragmentation into isolated vesicles or short tubules. Vacuolar degeneration due to cristae dilation: Intramitochondrial vacuoles with diameters exceeding 50 nm are classified as vacuolar damage [71,72].

4.12. Immunohistochemistry (IHC)

Human and murine skeletal muscle samples were sectioned at 4 μm, and stained for Dio3 (A6900, Abclonal, China), BNIP3 (A5683, Abclonal, China), FUNDC1 (28519-1-AP, proteintech, China), and PINK1 (23274-1-AP, proteintech, China), respectively. These sections were then incubated with a goat anti-rabbit IgG-HRP secondary antibody. A Digital Pathology Syestem captured the resultant images (3D-Histech, Pannoramic MIDI, Hungary).

4.13. Immunofluorescence (IF)

Human and murine skeletal muscle samples were sectioned and stained for LC3AB (12741, CST, USA), Tom20 (11802-1-AP, proteintech, China), MYH1(GB112130, Servicebio, China), and MYH7 (GB112131, Servicebio, China) by standard protocols. Nuclei were highlighted with DAPI counterstaining and imaged using a Digital Pathology Syestem captured the resultant images (3D-Histech, Pannoramic MIDI, Hungary). Differentiated C2C12 myoblasts were plated onto coverslips and stained for PINK1 (23274-1-AP, proteintech, China), Parkin (66674-1-Ig, proteintech, China), and Mitotracker (C1035, Beyotime, China) by standard protocols. The resultant images were captured by a laser-scanning confocal imaging system (Olympus, FV3000, Japan).

4.14. Immunofluorescence-based quantification of mitophagy

Immunofluorescence images were processed using CaseViewer software with standardized intensity adjustments (Black level: 6; Tom20: 40; LC3B: 30). Individual channel images were saved for analysis. In ImageJ, LC3B and Tom20 channels were converted to 8-bit, and a uniform threshold (40–255) was applied after cross-validation with raw images. Noise was removed by excluding particles $\leq$2 pixels (circularity: 0.5–1.0) using Analyze Particles. Colocalization was determined via the AND function in ROI Manager to identify overlapping LC3B/Tom20 signals. Mitophagy activity was calculated as the percentage of merged area relative to Tom20-positive area (Merged/Tom20 $\times$ 100), with six

random fields analyzed per image.

4.15. Immunoblotting

Immunoblotting analyses of tissue and cell lysates were conducted in accordance with a standardized protocol. Primary antibodies were applied at a dilution of recommended concentrations. Secondary antibodies, including goat anti-rabbit IgG-HRP (SA00001-2, Proteintech, China) and goat anti-mouse IgG-HRP (SA00001-1, Proteintech, China), were diluted to 1:20,000 in TBST. The immunoblots were visualized using a chemiluminescence detection system (Tanon, China). Subsequent densitometric quantification was carried out employing ImageJ software. A comprehensive list of the primary antibodies utilized in these experiments is presented in Table S1.

4.16. Real-time quantitative PCR (qRT-PCR)

RNA was extracted from rat tissues and C2C12 myoblasts utilizing the RNAeasy Animal Isolation Kit (R0026, Beyotime, China). Subsequently, cDNA was synthesized with the aid of Vazyme's reverse transcription kit (R323-01, Vazyme, China). The ensuing reverse transcription polymerase chain reaction (RT-PCR) was executed on an ABI 7500 platform, applying the ChamQ SYBR Color qPCR Master Mix (Q431-02, Vazyme, China) in conjunction with primers detailed in Supplementary Table S2. Quantitative analysis was performed by determining the Ct values and applying the comparative Ct (2^-ΔΔCT) method, with the housekeeping gene β-actin as a reference for normalization.

4.17. Co-immunoprecipitation (Co-IP)

Co-IP assays were executed utilizing the Pierce™ Magnetic Bead Co-IP Kit (88804, Thermo Scientific, USA). The procedure commenced with the preparation of C2C12 myoblast lysates, which were incubated with specific primary antibodies targeting Pan-acetylation (66289-1-Ig, Proteintech, China), PARL (26679-1-AP, Proteintech, China), or OMA1 (17116-1-AP, Proteintech, China). These lysates were then subjected to immunoprecipitation using Protein A + G Magnetic Beads. Once eluted from the magnetic beads, the precipitated complexes were subsequently evaluated by immunoblotting with antibodies specific to PINK1, Parkin, PARL, and OMA1, respectively.

4.18. Chromatin immunoprecipitation (ChIP)

The ChIP assay was carried out employing a commercially available enzymatic ChIP kit (P2083S, Beyotime, China). Nuclear lysates from C2C12 myoblasts, obtained after 1 % formaldehyde cross-linking, were subjected to sonication to shear chromatin. This was followed by immunoprecipitation using an antibody specific to THRα (ab53729, abcam, USA) or a non-specific IgG control. The enrichment of target genomic regions in both input and immunoprecipitated samples was assessed through conventional PCR and qRT-PCR. The PCR amplicons were resolved by electrophoresis on 2 % agarose gels, visualized with the BG-gdsAUTO550 gel imaging system (Baygene, China), and quantified utilizing ImageJ software. The primers designed for the putative THRα binding site within the NRK2 promoter sequence were as follows: forward primer 5′-TTCAGCAGTTACAGTAGAGG-3′ and reverse primer 5′-TATGTGTCTGTCGTCCAAG-3'.

4.19. Statistical analysis

Comprehensive statistical analyses were performed utilizing the sophisticated capabilities of GraphPad Prism 8.0 software. Prior to analysis, the assumptions of normality and homogeneity of variance were rigorously evaluated using the Shapiro-Wilk test and Levene's test, respectively. For evaluating differences across multiple groups, one-way ANOVA was employed, supplemented by Tukey's post-hoc test for delineating specific pairwise contrasts. For the comparison of binary outcomes, a standard *t*-test was applied. Correlative assessments were conducted using the Spearman's rank correlation analysis. Data presentation was optimized for clarity, with results depicted as mean ± SD for parametric data sets or through box-and-whisker plots for a visual representation of the distribution and variability. The threshold for statistical significance was set at $p < 0.05$.

CRediT authorship contribution statement

Gang Wang: Writing – review & editing, Writing – original draft, Visualization, Validation, Project administration, Methodology, Investigation, Formal analysis, Data curation, Conceptualization. **Ming Chen:** Writing – review & editing, Writing – original draft, Validation, Software, Project administration, Methodology, Investigation, Formal analysis, Data curation, Conceptualization. **Yuheng Zhang:** Writing – review & editing, Writing – original draft, Visualization, Validation, Methodology, Investigation, Formal analysis, Data curation, Conceptualization. **Dacheng Wang:** Validation, Investigation, Formal analysis, Data curation. **Tao Gao:** Visualization, Project administration, Methodology, Data curation, Conceptualization. **Jianfeng Duan:** Supervision, Software, Resources, Funding acquisition, Data curation, Conceptualization. **Huimin Lu:** Visualization, Validation, Investigation, Formal analysis, Data curation. **Minhua Cheng:** Supervision, Resources, Project administration, Investigation, Funding acquisition, Conceptualization. **Yun Xu:** Visualization, Validation, Investigation, Formal analysis, Data curation. **Xiaoyao Li:** Supervision, Software, Resources, Project administration, Funding acquisition, Formal analysis, Data curation. **Yan Wang:** Writing – review & editing, Supervision, Resources, Project administration, Methodology, Funding acquisition, Conceptualization. **Ke Cao:** Writing – review & editing, Writing – original draft, Validation, Supervision, Software, Resources, Project administration, Methodology, Investigation, Formal analysis, Data curation, Conceptualization. **Wenkui Yu:** Writing – review & editing, Writing – original draft, Validation, Supervision, Software, Resources, Project administration, Methodology, Investigation, Funding acquisition, Data curation, Conceptualization.

Ethics approval and consent to participate

All procedures of the animal experiments were approved by the Animal Research Committee of Nanjing University Medical School (2022AE02004). All skeletal muscle samples were collected with written informed consent from patients and following the guidelines approved by the ethics boards of the Nanjing Drum Tower Hospital (Ethics number: 2023-427-03).

Consent for publication

All authors have approved the publication of this manuscript.

Funding

This work was supported by the National Natural Science Foundation of China (Grant Nos. 81927808), China International Medical Foundation (N-2021-15-13), China Postdoctoral Science Foundation (Grant Nos. 2023M731635), The Young Scientists Fund of the National Natural Science Foundation of China (Grant Nos. 82302442). Natural Science Foundation of Jiangsu Province(Youth Project)BK20210026. Fundings for Clinical Trials from the Affiliated Drum Tower Hospital, Medical School of Nanjing University [Grant Nos. 2021-LCYJ-PY-40].

Declaration of competing interest

The authors declare that they have no known competing financial

interests or personal relationships that could have appeared to influence the work reported in this paper.

Appendix A. Supplementary data

Supplementary data to this article can be found online at https://doi.org/10.1016/j.redox.2025.103751.

Data availability

Data will be made available on request.

References

[1] M.M. Parker, Sepsis definitions: I know it when I see it, Crit. Care Med. 50 (2022) 148–150.
[2] K.R. Chadda, Z. Puthucheary, Persistent inflammation, immunosuppression, and catabolism syndrome (PICS): a review of definitions, potential therapies, and research priorities, Br. J. Anaesth. 132 (2024) 507–518.
[3] H.H. Zhou, Y. Liao, Z. Peng, et al., Association of muscle wasting with mortality risk among adults: a systematic review and meta-analysis of prospective studies, J. Cachexia Sarcopenia Muscle 14 (2023) 1596–1612.
[4] L. Evans, A. Rhodes, W. Alhazzani, et al., Surviving sepsis campaign: international guidelines for management of sepsis and septic shock 2021, Crit. Care Med. 49 (2021).
[5] D.K. Heyland, J. Patel, C. Compher, et al., The effect of higher protein dosing in critically ill patients with high nutritional risk (EFFORT Protein): an international, multicentre, pragmatic, registry-based randomised trial, Lancet 401 (2023) 568–576.
[6] I. Yoshihara, Y. Kondo, K. Okamoto, et al., Sepsis-associated muscle wasting: a comprehensive review from bench to bedside, Int. J. Mol. Sci. 24 (2023).
[7] Y. Wang, S. Tan, Q. Yan, et al., Sarcopenia and COVID-19 outcomes, Clin. Interv. Aging 18 (2023) 359–373.
[8] B. Biondi, G.J. Kahaly, R.P. Robertson, Thyroid dysfunction and diabetes mellitus: two closely associated disorders, Endocr. Rev. 40 (2019) 789–824.
[9] P. de Lange, R. Senese, F. Cioffi, et al., Rapid activation by 3,5,3'-L-triiodothyronine of adenosine 5'-monophosphate-activated protein kinase/acetyl-coenzyme a carboxylase and akt/protein kinase B signaling pathways: relation to changes in fuel metabolism and myosin heavy-chain protein content in rat gastrocnemius muscle in vivo, Endocrinology 149 (2008) 6462–6470.
[10] R. Mullur, Y.Y. Liu, G.A. Brent, Thyroid hormone regulation of metabolism, Physiol. Rev. 94 (2014) 355–382.
[11] C. Luongo, M. Dentice, D. Salvatore, Deiodinases and their intricate role in thyroid hormone homeostasis, Nat. Rev. Endocrinol. 15 (2019) 479–488.
[12] I. Vanhorebeek, I. Derese, J. Gunst, et al., Persisting neuroendocrine abnormalities and their association with physical impairment 5 years after critical illness, Crit. Care 25 (2021) 430.
[13] D. Salvatore, W.S. Simonides, M. Dentice, et al., Thyroid hormones and skeletal muscle–new insights and potential implications, Nat. Rev. Endocrinol. 10 (2014) 206–214.
[14] G. Wang, T. Gao, Y. Liu, et al., Type 3 deiodinase activation mediated by the Shh/Gli 1 axis promotes sepsis-induced metabolic dysregulation in skeletal muscles, Burns Trauma 13 (2025) tkae066.
[15] F. Cioffi, A. Giacco, F. Goglia, et al., Bioenergetic aspects of mitochondrial actions of thyroid hormones, Cells 11 (2022).
[16] K.L. Davies, E.J. Camm, E.V. Atkinson, et al., Development and thyroid hormone dependence of skeletal muscle mitochondrial function towards birth, J. Physiol. 598 (2020) 2453–2468.
[17] Y. Lei, M. Gan, Y. Qiu, et al., The role of mitochondrial dynamics and mitophagy in skeletal muscle atrophy: from molecular mechanisms to therapeutic insights, Cell. Mol. Biol. Lett. 29 (2024) 59.
[18] B.L. Baechler, D. Bloemberg, J. Quadrilatero, Mitophagy regulates mitochondrial network signaling, oxidative stress, and apoptosis during myoblast differentiation, Autophagy 15 (2019) 1606–1619.
[19] J.P. Leduc-Gaudet, D. Mayaki, O. Reynaud, et al., Parkin overexpression attenuates sepsis-induced muscle wasting, Cells 9 (2020).
[20] S. Sedraoui, J.P. Leduc-Gaudet, D. Mayaki, et al., Lack of compensatory mitophagy in skeletal muscles during sepsis, J. Physiol. 602 (2024) 2823–2838.
[21] S. Wang, H. Long, L. Hou, et al., The mitophagy pathway and its implications in human diseases, Signal Transduct. Targeted Ther. 8 (2023) 304.
[22] P. Terešak, A. Lapao, N. Subic, et al., Regulation of PRKN-independent mitophagy, Autophagy 18 (2022) 24–39.
[23] A. Picca, J. Faitg, J. Auwerx, et al., Mitophagy in human health, ageing and disease, Nat. Metab. 5 (2023) 2047–2061.
[24] L. Liu, K. Sakakibara, Q. Chen, et al., Receptor-mediated mitophagy in yeast and mammalian systems, Cell Res. 24 (2014) 787–795.
[25] J.P. Leduc-Gaudet, S.N.A. Hussain, E. Barreiro, et al., Mitochondrial dynamics and mitophagy in skeletal muscle health and aging, Int. J. Mol. Sci. 22 (2021).
[26] A.E. Vincent, Y.S. Ng, K. White, et al., The spectrum of mitochondrial ultrastructural defects in mitochondrial myopathy, Sci. Rep. 6 (2016) 30610.
[27] D.J. Klionsky, A.K. Abdel-Aziz, S. Abdelfatah, et al., Guidelines for the use and interpretation of assays for monitoring autophagy, Autophagy 17 (1) (2021) 1–382, 4th edition.
[28] G.S. Supinski, E.A. Schroder, L.A. Callahan, Mitochondria and critical illness, Chest 157 (2020) 310–322.
[29] W. Wasyluk, A. Zwolak, Metabolic alterations in sepsis, J. Clin. Med. 10 (2021).
[30] I.Y. Benador, M. Veliova, K. Mahdaviani, et al., Mitochondria bound to lipid droplets have unique bioenergetics, composition, and dynamics that support lipid droplet expansion, Cell Metab. 27 (2018) 869–885.e866.
[31] S. Sekine, R.J. Youle, PINK1 import regulation; a fine system to convey mitochondrial stress to the cytosol, BMC Biol. 16 (2018) 2.
[32] R.S. Fletcher, J. Ratajczak, C.L. Doig, et al., Nicotinamide riboside kinases display redundancy in mediating nicotinamide mononucleotide and nicotinamide riboside metabolism in skeletal muscle cells, Mol. Metabol. 6 (2017) 819–832.
[33] L. Wang, H. Qi, Y. Tang, et al., Post-translational modifications of key machinery in the control of mitophagy, Trends Biochem. Sci. 45 (2020) 58–75.
[34] C. Meissner, H. Lorenz, B. Hehn, et al., Intramembrane protease PARL defines a negative regulator of PINK1- and PARK2/Parkin-dependent mitophagy, Autophagy 11 (2015) 1484–1498.
[35] S. Sekine, C. Wang, D.P. Sideris, et al., Reciprocal roles of Tom 7 and OMA1 during mitochondrial import and activation of PINK1, Mol. Cell 73 (2019) 1028–1043.e1025.
[36] A. Cercillieux, E. Ciarlo, C. Canto, Balancing NAD(+) deficits with nicotinamide riboside: therapeutic possibilities and limitations, Cell. Mol. Life Sci. 79 (2022) 463.
[37] S.E. Jolley, A.E. Bunnell, C.L. Hough, ICU-acquired weakness, Chest 150 (2016) 1129–1140.
[38] J.C. Preiser, C. Ichai, J.C. Orban, et al., Metabolic response to the stress of critical illness, Br. J. Anaesth. 113 (2014) 945–954.
[39] V.E. Polcz, E.L. Barrios, S.D. Larson, et al., Charting the course for improved outcomes in chronic critical illness: therapeutic strategies for persistent inflammation, immunosuppression, and catabolism syndrome (PICS), Br. J. Anaesth. 133 (2024) 260–263.
[40] I. Vanhorebeek, N. Latronico, G. Van den Berghe, ICU-acquired weakness, Intensive Care Med. 46 (2020) 637–653.
[41] M.C. Cox, M. Booth, G. Ghita, et al., The impact of sarcopenia and acute muscle mass loss on long-term outcomes in critically ill patients with intra-abdominal sepsis, J. Cachexia Sarcopenia Muscle 12 (2021) 1203–1213.
[42] S.A. McClave, R.G. Martindale, V.W. Vanek, et al., Guidelines for the provision and assessment of nutrition support therapy in the adult critically ill patient: society of critical care medicine (SCCM) and American society for parenteral and enteral nutrition (A.S.P.E.N.), JPEN - J. Parenter. Enter. Nutr. 33 (2009) 277–316.
[43] P. Singer, A.R. Blaser, M.M. Berger, et al., ESPEN guideline on clinical nutrition in the intensive care unit, Clin. Nutr. 38 (2019) 48–79.
[44] E. Fliers, A.C. Bianco, L. Langouche, et al., Thyroid function in critically ill patients, Lancet Diabetes Endocrinol. 3 (2015) 816–825.
[45] H. Chang, C. Lin, Z. Li, et al., T3 alleviates neuroinflammation and reduces early brain injury after subarachnoid haemorrhage by promoting mitophagy via PINK 1-parkin pathway, Exp. Neurol. 357 (2022) 114175.
[46] W. Bi, J. Jia, R. Pang, et al., Thyroid hormone postconditioning protects hearts from ischemia/reperfusion through reinforcing mitophagy, Biomed. Pharmacother. 118 (2019) 109220.
[47] Y. Martínez, X. Li, G. Liu, et al., The role of methionine on metabolism, oxidative stress, and diseases, Amino Acids 49 (2017) 2091–2098.
[48] L. Meng, C. Lu, B. Wu, et al., Taurine antagonizes macrophages M1 polarization by mitophagy-glycolysis switch blockage via dragging SAM-PP2Ac transmethylation, Front. Immunol. 12 (2021) 648913.
[49] C.J. Fowler, Oleamide: a member of the endocannabinoid family? Br. J. Pharmacol. 141 (2004) 195–196.
[50] A. Parada-Bustamante, C. Valencia, P. Reuquen, et al., Role of 2-methoxyestradiol, an endogenous estrogen metabolite, in health and disease, Mini Rev. Med. Chem. 15 (2015) 427–438.
[51] C. Perez-Stable, 2-Methoxyestradiol and paclitaxel have similar effects on the cell cycle and induction of apoptosis in prostate cancer cells, Cancer Lett. 231 (2006) 49–64.
[52] Y.S. Elhassan, K. Kluckova, R.S. Fletcher, et al., Nicotinamide riboside augments the aged human skeletal muscle NAD(+) metabolome and induces transcriptomic and anti-inflammatory signatures, Cell Rep. 28 (2019) 1717–1728.e1716.
[53] H.A.K. Lapatto, M. Kuusela, A. Heikkinen, et al., Nicotinamide riboside improves muscle mitochondrial biogenesis, satellite cell differentiation, and gut microbiota in a twin study, Sci. Adv. 9 (2023) eadd5163.
[54] M. Song, S.H. Armenian, R. Bhandari, et al., Exercise training and NR supplementation to improve muscle mass and fitness in adolescent and young adult hematopoietic cell transplant survivors: a randomized controlled trial {1, BMC Cancer 22 (2022) 795.
[55] C. Cantó, R.H. Houtkooper, E. Pirinen, et al., The NAD(+) precursor nicotinamide riboside enhances oxidative metabolism and protects against high-fat diet-induced obesity, Cell Metab. 15 (2012) 838–847.
[56] T. Wei, G. Huang, J. Gao, et al., Sirtuin 3 deficiency accelerates hypertensive cardiac remodeling by impairing angiogenesis, J. Am. Heart Assoc. 6 (2017).
[57] S. Liu, Y. Liu, J. Li, et al., Arsenic exposure-induced acute kidney injury by regulating SIRT1/PINK1/mitophagy Axis in mice and in HK-2 cells, J. Agric. Food Chem. 71 (2023) 15809–15820.
[58] C. Yan, L. Gong, L. Chen, et al., PHB2 (prohibitin 2) promotes PINK1-PRKN/Parkin-dependent mitophagy by the PARL-PGAM5-PINK1 axis, Autophagy 16 (2020) 419–434.

[59] S. Akabane, K. Watanabe, H. Kosako, et al., TIM23 facilitates PINK1 activation by safeguarding against OMA1-mediated degradation in damaged mitochondria, Cell Rep. 42 (2023) 112454.
[60] X.R. Yang, R. Wen, N. Yang, et al., Role of sirtuins in sepsis and sepsis-induced organ dysfunction: a review, Int. J. Biol. Macromol. 278 (2024) 134853.
[61] J. Guo, Y. Shi, X. Yu, et al., THRA1/PGC-1α/SIRT3 pathway regulates oxidative stress and is implicated in hypertension of maternal hypothyroid rat offspring, Hypertens. Res. 48 (2025) 1080–1098.
[62] I. López-Mateo, D. Rodríguez-Muñoz, J.V. de La Rosa, et al., Regulation of metabolic and transcriptional responses by the thyroid hormone in cellular models of murine macrophages, Front. Immunol. 13 (2022) 923727.
[63] M. Ye, Y. Zhao, Y. Wang, et al., NAD(H)-loaded nanoparticles for efficient sepsis therapy via modulating immune and vascular homeostasis, Nat. Nanotechnol. 17 (2022) 880–890.
[64] J. Yoshino, J.A. Baur, S.I. Imai, NAD(+) intermediates: the biology and therapeutic potential of NMN and NR, Cell Metab. 27 (2018) 513–528.
[65] G.F.S. Alegre, G.M. Pastore, NAD+ precursors nicotinamide mononucleotide (NMN) and nicotinamide riboside (NR): potential dietary contribution to health, Curr. Nutr. Rep. 12 (2023) 445–464.
[66] G.J. Zhao, X.Y. Yang, C. Zhang, et al., Supplementation with nicotinamide riboside attenuates T cell exhaustion and improves survival in sepsis, Shock 60 (2023) 238–247.
[67] G. Hong, D. Zheng, L. Zhang, et al., Administration of nicotinamide riboside prevents oxidative stress and organ injury in sepsis, Free Radic. Biol. Med. 123 (2018) 125–137.
[68] M. Dentice, R. Ambrosio, V. Damiano, et al., Intracellular inactivation of thyroid hormone is a survival mechanism for muscle stem cell proliferation and lineage progression, Cell Metab. 20 (2014) 1038–1048.
[69] G.W. Rogers, M.D. Brand, S. Petrosyan, et al., High throughput microplate respiratory measurements using minimal quantities of isolated mitochondria, PLoS One 6 (2011) e21746.
[70] A.S. Divakaruni, W.Y. Hsieh, L. Minarrieta, et al., Etomoxir inhibits macrophage polarization by disrupting CoA homeostasis, Cell Metab. 28 (2018) 490–503.e497.
[71] E.P. Bulthuis, M.J.W. Adjobo-Hermans, P. Willems, et al., Mitochondrial morphofunction in mammalian cells, Antioxidants Redox Signal. 30 (2019) 2066–2109.
[72] T.G. Frey, C.A. Mannella, The internal structure of mitochondria, Trends Biochem. Sci. 25 (2000) 319–324.